Atmos. Chem. Phys., 16, 12099–12125, 2016
www.atmos-chem-phys.net/16/12099/2016/
doi:10.5194/acp-16-12099-2016

Atmospheric Chemistry and Physics Open Access EGU

Modeling the reactive halogen plume from Ambrym and its impact on the troposphere with the CCATT-BRAMS mesoscale model

Line Jourdain[1], **Tjarda Jane Roberts**[1], **Michel Pirre**[1], **and Beatrice Josse**[2]

[1]Laboratoire de Physique et de Chimie de l'Environnement et de l'Espace (LPC2E), Université d'Orléans, CNRS, Orléans, France
[2]CNRM-GAME, Météo-France and CNRS, Toulouse, France

Correspondence to: Line Jourdain (line.jourdain@cnrs-orleans.fr)

Received: 31 July 2015 – Published in Atmos. Chem. Phys. Discuss.: 16 December 2015
Revised: 4 August 2016 – Accepted: 8 August 2016 – Published: 28 September 2016

Abstract. Ambrym Volcano (Vanuatu, southwest Pacific) is one of the largest sources of continuous volcanic emissions worldwide. As well as releasing SO_2 that is oxidized to sulfate, volcanic plumes in the troposphere are shown to undergo reactive halogen chemistry whose atmospheric impacts have been little explored to date. Here, we investigate with the regional-scale model CCATT-BRAMS (Coupled Chemistry Aerosol-Tracer Transport model, Brazilian developments on the Regional Atmospheric Modeling System, version 4.3) the chemical processing in the Ambrym plume and the impact of this volcano on the atmospheric chemistry on both local and regional scales. We focus on an episode of extreme passive degassing that occurred in early 2005 and for which airborne DOAS (differential optical absorption spectroscopy) measurements of SO_2 and BrO columns in the near-downwind plume between 15 and 40 km from the vents have been reported. The model was developed to include reactive halogen chemistry and a volcanic emission source specific to this extreme degassing event. In order to test our understanding of the volcanic plume chemistry, we performed very high-resolution (500 m × 500 m) simulations using the model nesting grid capability and compared each DOAS measurement to its temporally and spatially interpolated model counterpart "point-by-point". Simulated SO_2 columns show very good quantitative agreement with the DOAS observations, suggesting that the plume direction as well as its dilution in the near-downwind plume are well captured. The model also reproduces the salient features of volcanic chemistry as reported in previous work, such as HO_x and ozone depletion in the core of the plume. When a high-temperature chemistry initialization is included, the model is able to capture the observed BrO / SO_2 trend with distance from the vent. The main discrepancy between observations and model is the bias between the magnitudes of observed and simulated BrO columns that ranges from 60 % (relative to the observations) for the transect at 15 km to 14 % for the one at 40 km from the vents. We identify total in-plume depletion of ozone as a limiting factor for the partitioning of reactive bromine into BrO in the near-source (concentrated) plume under these conditions of extreme emissions and low background ozone concentrations (15 ppbv). Impacts of Ambrym in the southwest Pacific region were also analyzed. As the plume disperses regionally, reactive halogen chemistry continues on sulfate aerosols produced by SO_2 oxidation and promotes BrCl formation. Ozone depletion is weaker than on the local scale but still between 10 and 40 % in an extensive region a few thousands of kilometers from Ambrym. The model also predicts the transport of bromine to the upper troposphere and stratosphere associated with convection events. In the upper troposphere, HBr is reformed from Br and HO_2. Comparison of SO_2 regional-scale model fields with OMI (Ozone Monitoring Instrument) satellite SO_2 fields confirms that the Ambrym SO_2 emissions estimate based on the DOAS observations used here is realistic.

The model confirms the potential of volcanic emissions to influence the oxidizing power of the atmosphere: methane lifetime (calculated with respect to OH and Cl) is increased overall in the model due to the volcanic emissions. When considering reactive halogen chemistry, which depletes HO_x and ozone, the lengthening of methane lifetime with respect to OH is increased by a factor of 2.6 compared to a simulation including only volcanic SO_2 emissions. Cl radicals

produced in the plume counteract 41 % of the methane lifetime lengthening due to OH depletion. Including the reactive halogen chemistry in our simulation also increases the lifetime of SO_2 in the plume with respect to oxidation by OH by 36 % compared to a simulation including only volcanic SO_2 emissions. This study confirms the strong influence of Ambrym emissions during the extreme degassing event of early 2005 on the composition of the atmosphere on both local and regional scales. It also stresses the importance of considering reactive halogen chemistry when assessing the impact of volcanic emissions on climate.

1 Introduction

Volcanic activity is a source of climatically and environmentally important gases and aerosols in the atmosphere. In this context, much work has focused on the climate impact of sulfur compounds injected by major volcanic explosions into the stratosphere. In this layer, they are converted into sulfate aerosols that have a long residence time ($\sim$ 1–2 years) and can affect climate directly via the perturbation of the Earth's radiation balance as well as indirectly due to the strong coupling between radiation, microphysics and atmospheric chemistry in the stratosphere. This forcing from volcanic stratospheric aerosols is now well understood and is thought to be the most important natural cause of externally forced climate change on annual but also on multi-decadal timescales and hence is thought to explain the majority of the preindustrial climate change of the last millennium (Myhre et al., 2013).

On the other hand, the impact of other compounds as halides (HCl, HBr) injected by explosive eruptions into the stratosphere as well as the overall impact of minor eruptions and quiescent passive degassing have been largely overlooked. However, the presence of volcanic halogens in the stratosphere following explosive eruptions has recently been detected (e.g., Hunton et al., 2005; Rose et al., 2006; Prata et al., 2007; Theys et al., 2014; Carn et al., 2016). Such volcanic halogen injection, enabled by incomplete volcanic halide washout as first predicted by a model study (Textor et al., 2003), was found to cause enhanced reactive chlorine and bromine as well as enhanced ozone depletion (Rose et al., 2006; Millard et al., 2006). As a result, it is important, as emphasized in Cadoux et al. (2015), to consider volcanic halogens in addition to sulfur compounds when studying the influence of past and future explosive eruptions on the stratosphere.

Until recently, the impact of quiescent degassing and of minor eruptions has also been largely overlooked because of the lower lifetime of volcanic emissions in the troposphere. However, it has been shown that quiescent degassing alone is responsible for a high proportion ($\sim$ 30–70 %) of the volcanic SO_2 flux to the atmosphere (Andres and Kasgnoc, 1998; Halmer et al., 2002; Mather et al., 2003). In addition, quiescent degassing as well as minor eruptions were found to contribute more to the sulfur load in the free troposphere with regard to their emissions compared to stronger oceanic and anthropogenic sources due to the elevation of most volcanoes (e.g., Chin and Jacob, 1996; Graf et al., 1997). Furthermore, recent studies show the need for a better knowledge of the tropospheric concentrations of natural aerosols and their precursor gases to quantify the aerosol indirect forcing from anthropogenic activities due to nonlinearities in the relations linking aerosol concentrations and cloud albedo (Carslaw et al., 2013; Schmidt et al., 2012). Volcanic emissions in the troposphere have also been recognized to cause environmental and health problems due to the deposition of SO_2, sulfate, hydrogen halides (mainly HCl and HF) and toxic metals (for a review, see Delmelle, 2003) as well as adversely impacting air quality.

Finally, there is also evidence of chemical reactivity in tropospheric plumes with consequences for the oxidizing power of the troposphere (and hence effects on climate) as well as for the deposition of mercury (e.g., von Glasow, 2010). Indeed, reactive halogens such as BrO (e.g., Bobrowski et al., 2003, 2015; Lee et al., 2005; Oppenheimer et al., 2006; Bobrowski and Platt, 2007; Bani et al., 2009; Kern et al., 2009; Theys et al., 2009; Boichu et al., 2011; Kelly et al., 2013; Hörmann et al., 2013) as well as OClO (Bobrowski et al., 2007; General et al., 2015; Gliß et al., 2015) have been detected in the plumes of many volcanoes worldwide. Observations of ClO have also been reported (Lee et al., 2005) but are subject to some uncertainties (see Roberts et al., 2009). For BrO, it is clear that its formation results from the conversion of the emitted volcanic HBr gas into reactive bromine in the presence of sulfate aerosols (Oppenheimer et al., 2006; Bobrowski et al., 2007; Roberts et al., 2009; von Glasow, 2010). Central to this chemical mechanism, first identified in the context of arctic spring ozone depletion events (Fan and Jacob, 1992), is the reactive uptake of HOBr on the sulfate aerosol. The net result is the release of gaseous reactive bromine from the sulfate aerosol (initially as Br_2, which then converts into other forms including Br, BrO, HOBr and $BrONO_2$) and the depletion of the oxidants O_3, HO_2 and NO_2. Reactive bromine acts as a catalyst for its own formation, leading to an exponential growth called "bromine explosion" also observed in the arctic during spring (e.g., Barrie et al., 1988), in the marine boundary layer (e.g., Saiz-Lopez et al., 2004) and over salt lakes (e.g., Hebestreit et al., 1999) (for a review see Simpson et al., 2015). Following the first discovery of volcanic BrO (Bobrowski et al., 2003), the depletion of ozone has also been observed in volcanic plumes (Vance et al., 2010; Oppenheimer et al., 2010; Schuman et al., 2011; Kelly et al., 2013; Surl et al., 2015). The plume atmospheric chemistry is also highly influenced by the degree of plume mixing with entrained ambient air (Roberts et al., 2014a).

Owing to the numerous environmental and climate impacts of quiescent degassing and minor eruptions occurring in the troposphere, it is important to take these volcanic sources into account in the 3-D atmospheric models (regional and global models) that aim to understand the chemical composition of the atmosphere, its evolution and its interaction with climate. This paper is an attempt to do that and builds on previous modeling work. The numerical 1-D models MISTRA and PlumeChem (e.g., Bobrowski et al., 2007; Roberts et al., 2009, 2014a; von Glasow, 2010; Boichu et al., 2011; Kelly et al., 2013) are able to broadly reproduce observed ratios of BrO to SO_2 with distance downwind from volcanoes as well as simulate ozone depletion (e.g., Roberts et al., 2014a; Surl et al., 2015). These modeling studies show the need to take into account the high-temperature chemistry following the mixing of volcanic gas with ambient air in order to reproduce the timing of BrO formation. Indeed, high-temperature model studies (Gerlach, 2004; Martin et al., 2006, 2009) have predicted that the mixing of volcanic gases and air at the vent leads to high-temperature oxidative dissociation and hence to the formation of radical species. These species accelerate the onset of this chemistry, the formation of BrO being autocatalytical and driven forwards by low-temperature reactions occurring on volcanic aerosol. To date, simulations of reactive halogen (BrO_x, ClO_x) chemistry in volcanic plumes and its impacts have been restricted to 1-D and box model studies.

Here, we present a 3-D regional model study of the impact of Ambrym Volcano emissions (not only of sulfur emissions but also of halogen emissions including their reactive chemistry) on the chemical composition of the troposphere on both local and regional scales. Ambrym Volcano, Vanuatu, is recognized as a significant contributor to the global volcanic flux of SO_2 (Bani et al., 2012; Allard et al., 2009, 2015) and of the halogen halides HF, HCl and HBr (Allard et al., 2009, 2015). Our focus is an extreme degassing episode that occurred in early 2005, for which airborne DOAS (differential optical absorption spectroscopy) SO_2 and BrO columns in the plume (15–40 km of the vents) have been reported (Bani et al., 2009).

The paper is organized as follows. In Sect. 2, we briefly present Ambrym Volcano and the main chemical reactions of volcanic plumes. We also present the reported measurements and detail the model developments made in this study. In Sect. 3, we first test our understanding of the plume chemistry at the plume level by comparing the model fields with the DOAS SO_2 and BrO columns in the near-downwind plume "point-by-point" as well as by performing some sensitivity studies. The local impact of the Ambrym plume is also presented. In Sect. 4, the regional impact of the Ambrym plume is analyzed and discussed. The conclusions are presented in Sect. 5.

2 Methods

2.1 The context: Ambrym Volcano and volcanic plume chemistry

2.1.1 Ambrym Volcano

The Vanuatu Arc is a group of about 80 islands and islets located in the southwest Pacific that was formed and continued to evolve as a result of the complex interaction between the Pacific plate and the Indo-Australian plate (Robin et al., 1993). Ambrym (160°08′ E, 16°15′ S), situated in the central zone of the Vanuatu Arc, is a basaltic stratovolcano 35×50 km wide, rising 1334 m above sea level (m a.s.l.). It has at its center a 12 km diameter caldera with two active cones, mounts Marum and Benbow, filled with permanent lava lakes. It has recently been highlighted that the Vanuatu Arc is one of the most important entry points for volcanic gases into the atmosphere, with a mean annual emission of 3 Tg year^{-1} of SO_2 estimated for the period 2004–2009 representing about 20 % of the global volcanic SO_2 annual emissions (Bani et al., 2012). Under normal quiescent degassing conditions, Ambrym Volcano has a mean emission of 5.44 kt day^{-1} of SO_2, comparable with Mt Etna (Italy), and hence contributes to two thirds of the total budget of the arc (Bani et al., 2012). It is also a significant contributor to the global volcanic flux for several other species (Allard et al., 2009, 2015). The volcano impact on the population and environment includes crop damage and food shortages due to the deposition of halogen acids, SO_2 and H_2SO_4 as well as dental fluorosis due to the water contamination by the wet deposition of fluorine (Allibone et al., 2010). The volcano impact on sulfate aerosol in the southwest Pacific has also recently been investigated (Lefèvre et al., 2015). Lefèvre et al. (2015) found a strong signal in the aerosol optical depth (AOD) from MODIS (Moderate Resolution Imaging Spectroradiometer) due to Ambrym sulfur emissions; this signal contributes 15 % to the total AOD as far as 1500 km from the volcano. Here, we focus on the halogen impact alongside sulfur. We study an event of extreme passive degassing that took place in January 2005 when the SO_2 emission was more than 3 times higher than its mean value over the 2004–2009 period (Bani et al., 2012). This extreme degassing occurred as a pulse of several months' duration (Bani et al., 2012). Our study evaluates impacts from the continuous degassing on 12 January, enabling a comparison to plume BrO and SO_2 measurements from a field campaign (Bani et al., 2009).

2.1.2 Volcanic plume chemistry

Reactions (R1)–(R7) illustrate the autocatalytic conversion of volcanic HBr into reactive bromine species and the associated catalytic ozone depletion (for a more complete set of reactions, see Simpson et al., 2007). A key reaction is the heterogeneous reaction of HOBr with Br^- (from dissolved

volcanic HBr) and H^+ in volcanic sulfate aerosols (Reaction R1) that results in the production of Br_2. Once released to the gas phase, Br_2 is rapidly photolyzed to give two Br radicals (Reaction R2), which can react with ozone to form BrO (Reaction R3). The reaction of BrO with HO_2 (Reaction R5) re-forms HOBr, which can again react on the sulfate aerosol (Reaction R1) to further propagate the cycle, each time doubling the concentration of reactive bromine. In addition to the reactive uptake of HOBr, the hydrolysis of $BrONO_2$ (Reaction R7) into sulfate aerosol can also regenerate HOBr, which can undergo another cycle.

$$HOBr_{(aq)} + Br^-_{(aq)} + H^+_{(aq)} \rightarrow Br_{2(aq\rightarrow g)} + H_2O_{(l)} \quad (R1)$$

$$Br_2 \xrightarrow{h\nu} 2Br \quad (R2)$$

$$Br + O_3 \rightarrow BrO + O_2 \quad (R3)$$

$$BrO + BrO \rightarrow 2Br + O_2 \quad (R4a)$$

$$BrO + BrO \rightarrow Br2 + O_2 \quad (R4b)$$

$$BrO + HO_2 \rightarrow HOBr + O_2 \quad (R5)$$

$$BrO + NO_2 \rightarrow BrONO_2 \quad (R6)$$

$$BrONO_2 + H_2O_{(l)} \rightarrow HOBr + HNO_3 \quad (R7)$$

Because BrO can be photolyzed and the resulting O quickly reacts with O_2 to produce O_3, the key ozone destruction steps are Reaction (R3) together with Reactions (R4a), (R4b), (R5) and (R6) (von Glasow et al., 2009). Note, that BrCl can be the product of the reactive uptake of HOBr (Reaction R8) when Br^- becomes depleted, leading to non-autocatalytic formation of reactive chlorine.

$$HOBr_{(aq)} + H^+_{(aq)} + Cl^-_{(aq)} \rightarrow BrCl_{(aq\rightarrow g)} + H_2O_{(l)} \quad (R8)$$

2.2 Measurements

2.2.1 DOAS data

We use DOAS measurement of SO_2 and BrO columns performed in the plume of Ambrym during the episode of extreme passive degassing: the 12 January 2005 (Bani et al., 2009). The measurements were made between 05:00 and 06:00 UTC onboard of an aircraft flying just below the Ambrym plume (at 500–1000 m a.s.l.) in the crosswind direction (15–40 km southeast of the craters) with the instrument's telescope pointing to zenith. The procedure to retrieve the columns is described in Bani et al. (2009) and Bani et al. (2012). Reported errors (2σ) on the SO_2 and BrO retrieved columns are, respectively, $\pm 52\,mg\,m^{-2}$ (i.e., 4.89×10^{16} molecules cm^{-2}) and $\pm 0.39\,mg\,m^{-2}$ (i.e., 2.44×10^{14} molecules cm^{-2}). In the present study, these data are used to evaluate the simulation of volcanic plume chemistry. Note that these data in conjunction with wind estimates were used by Bani et al. (2009) to estimate the Ambrym SO_2 emission rate ($18.8\,kt\,day^{-1}$).

2.2.2 OMI data

The Ozone Monitoring Instrument (OMI) is a nadir viewing UV/visible CCD (charge-coupled device) spectrometer sampling a swath of 2600 km with a ground footprint of 13 km × 24 km, launched aboard the NASA Aura satellite in July 2004 (Bhartia and Wellemeyer, 2002). Here, we use the planetary boundary layer (PBL) level-2 SO_2 column amount product derived with the principal component analysis (PCA) algorithm (Li et al., 2013). Only data with scenes near the center of the swath (rows 5–55) with a radiative cloud fraction less than 0.3 and with an ozone slant column lower than 1500 DU were considered as recommended. Noise and biases in retrievals are estimated at ~ 0.5 DU for regions between 30° S and 30° N.

2.2.3 MODIS data

MODIS was launched aboard the NASA's Aqua satellite in May 2002. The MODIS instrument measures spectral radiances in 36 high spectral resolution bands between 410 and 14 400 nm, sampling a swath of 2330 km (Remer et al., 2008). We used the aerosol optical depth at 550 nm for both the ocean and the land product, derived from the 8-day average of global $1° \times 1°$ gridded daily level-3 products from MODIS Aqua (MYD08_E3 Collection 5.1). MODIS AOD is derived using algorithms detailed in Remer et al. (2005). Over oceans, MODIS AOD (τ) uncertainties have been shown to be about $\pm(0.03 + 0.05\tau)$; over land retrieval uncertainties are generally $\pm(0.05 + 0.15\tau)$ (Remer et al., 2008). It is important to note that we had to use the 8-day average AOD product because the daily files had too much missing data due to the presence of clouds in the Vanuatu region.

2.3 Model description and simulations

We use the CCATT-BRAMS (Coupled Chemistry Aerosol-Tracer Transport model, Brazilian developments on the Regional Atmospheric Modeling System, version 4.3) non-hydrostatic regional atmospheric chemistry model (described in detail in Longo et al., 2013). It is based on the Regional Atmospheric Modeling System (RAMS) developed by the University of Colorado for a range of applications: from large-eddy simulations in the planetary boundary layer to operational weather forecasting and climate studies (Walko et al., 2000). BRAMS builds upon RAMS and includes modifications and new features to improve the model performances within the tropics (Freitas et al., 2009). The parameterizations of physical processes such as surface–air exchanges, turbulence, convection, radiation and cloud microphysics are described in Freitas et al. (2009) and in Longo et al. (2013). BRAMS is coupled online to CCATT, which enables the transport, chemical evolution, emission and deposition of chemical and aerosol species (Longo et al., 2013). Note that

Table 1. Heterogeneous reactions in the model and their associated reactive uptake coefficients on sulfate aerosol. See Sect. 2.3.1 for description of the calculation of the ratio $[BrCl_{(aq)}]$ / $[Br_{2(aq)}]$.

Reaction	Reactive uptake coefficient
$HOBr + H^+_{(aq)} + Br^-_{(aq)} \rightarrow Br_{2(aq\rightarrow g)} + H_2O$	$0.2 \times \frac{[Br_{2(aq)}]}{[Br_{2(aq)}]+[BrCl_{(aq)}]}$
$HOBr + H^+_{(aq)} + Cl^-_{(aq)} \rightarrow BrCl_{(aq\rightarrow g)} + H_2O$	$0.2 \times \frac{[BrCl_{(aq)}]}{[Br_{2(aq)}]+[BrCl_{(aq)}]}$
$BrONO_2 + H_2O \rightarrow HOBr_{(aq\rightarrow g)} + HNO_3$	0.8

when BRAMS and CCATT are coupled, as in the present study, the prognostic chemical fields O_3, N_2O, CO_2 and CH_4 are used in the radiation scheme. The model has already been used to study regional air pollution, for instance the South America regional smoke plume (Rosário et al., 2013) and ozone production and transport over the Amazon Basin (Bela et al., 2015). It has also been used to assess the transport of tropospheric tracers by tropical convection (Arteta et al., 2009a, b) and for understanding the budget of bromoform (Marécal et al., 2012).

The CCATT model is described in detail by Longo et al. (2013). Here we focus on the particular settings of the model we used and the changes we made for the study.

2.3.1 Model chemistry

Within the CCATT model, we use the RACM chemistry scheme (Regional Atmospheric chemistry Mechanism; Stockwell et al., 1997) including 88 species and 237 chemical reactions and designed to study tropospheric chemistry from urban to remote conditions. Photolysis rates are calculated online during the simulation to take into account the presence of aerosols and clouds using Fast-TUV (Tropospheric Ultraviolet and Visible radiation model; Tie et al., 2003; Longo et al., 2013). The sulfur scheme includes gas-phase oxidation and dry and wet deposition but not aqueous-phase oxidation. In order to simulate halogen chemistry in volcanic plumes, we have added 16 halogen species and 54 reactions to the chemical scheme including photolysis and gas-phase and heterogeneous reactions. The gas-phase constant rates and photolysis cross sections are from the Jet Propulsion Laboratory (Sander et al., 2006) and the International Union of Pure and Applied Chemistry (Atkinson et al., 2007). The heterogeneous reactions include the hydrolysis of $BrONO_2$ and the reaction of $HOBr + X^-_{(aq)} + H^+_{(aq)}$, where $X = Br$ or Cl on sulfate aerosol. They are treated here with a reactive uptake formulation (Table 1) with a constant uptake coefficient. Ongoing developments are being made to prescribe a variable reactive uptake coefficient for HOBr as a function of the underlying gas–aerosol reaction kinetics, building on a recent reevaluation (Roberts et al., 2014b).

For the heterogeneous reaction of $HOBr_{(g)}$ with $X^-_{(aq)}$ where $X = Br$ or Cl, there is a subsequent interconversion between the products Br_2 and BrCl within the aerosols, based on the equilibria (Wang et al., 1994):

$$BrCl_{(aq)} + Br^-_{(aq)} \overset{K_1}{\longleftrightarrow} Br_2Cl^-_{(aq)}, \quad (1)$$

$$Br_2Cl^-_{(aq)} \overset{K_2}{\longleftrightarrow} Br_{2(aq)} + Cl^-_{(aq)}. \quad (2)$$

As a result, the relative amount of Br_2 and BrCl produced and released into the atmosphere depends on the equilibrium established by these two reactions. The Br_2 / BrCl ratio is given by Eq. (3) (derived from equilibria of Wang et al., 1994):

$$\frac{[Br_{2(aq)}]}{[BrCl_{(aq)}]} = \frac{K_1}{K_2}\frac{[Br^-_{(aq)}]}{[Cl^-_{(aq)}]}, \quad (3)$$

where the equilibrium constants of Eqs. (1) and (2) are $K_1 = 1.8\times10^4\,M^{-1}$ and $K_2 = 1.3\,M^{-1}$, respectively, and the amounts of $[Br^-]$ and $[Cl^-]$ in the aqueous phase are determined by the effective Henry's law constants (taken from Sander, 1999). We thus parameterize the reactive uptake coefficient of HOBr as two competing reactions (with Br^- and Cl^-) and, on the basis of Eq. (3), apply a branching ratio to the constant rates of reactions as shown in Table 1. This approach is the same as that proposed by Grellier et al. (2014) and also similar to Roberts et al. (2014a), who showed competition between Br_2 and BrCl as products from HOBr reactive uptake, finding that Br_2 is initially formed but BrCl becomes more prevalent once HBr becomes depleted. Note that heterogeneous reactions involving HOCl and $ClONO_2$ are slow compared to the reactions involving HOBr and $BrONO_2$ and are not taken into account in the model.

2.3.2 Sulfate aerosol surface density

In the model, sulfuric acid H_2SO_4 is a prognostic variable and assumed to be entirely in the aerosol phase. It is both directly emitted by the volcano (see Sect. 2.3.3 for details) and produced by the reaction of SO_2 with OH in the gas phase. We assume to have only binary H_2SO_4–H_2O aerosol. The weight percent of H_2SO_4 in the aerosol (wt) and the density of aerosols (ρ_{aer}) are calculated with the analytical expression of Tabazadeh et al. (1997), depending on the temperature and relative humidity. The total volume of aerosol V_{aer} (per cm^3) can then be calculated from H_2SO_4 concentrations, wt and ρ_{aer}. Few observations of volcanic aerosol size distribution exist, and none have been reported for Am-

Table 2. SO_2 emission rates in January 2005 from the principal active volcanoes on Vanuatu (Gaua, Aoba, Lopévi, Épi, Ambrym, Yasur) as prescribed in the simulations. Details for each volcano are given in the footnotes to the table.

Volcano	Reported activity	Emission ($kt\,day^{-1}$)	Source
Gaua	None	$0.070\,kt\,day^{-1}$	AEROCOM database[a]
Aoba (Ambae)	None	$0.070\,kt\,day^{-1}$	AEROCOM database[b]
Ambrym	Extreme passive degassing	$18.835\,kt\,day^{-1}$	Bani et al. (2012)[c]
Lopévi	Not clear	$0.070\,kt\,day^{-1}$	AEROCOM database[d]
Épi	None	$0.070\,kt\,day^{-1}$	AEROCOM database[e]
Yasur	Eruption	$0.968\,kt\,day^{-1}$	Bani et al. (2012)[f]

[a] In Bani et al. (2012), only information regarding a phase of eruptive activity is given. We prescribed the post-eruptive degassing rate (for the volcanoes that have erupted since 1900) of $0.070\,kt\,day^{-1}$ assigned for this volcano in the AEROCOM database. [b] Before the eruption of November 2005, there was no significant passive degassing. We prescribed the post-eruptive degassing rate of $0.070\,kt\,day^{-1}$ assigned in the AEROCOM database. [c] Mean of five transverses of 12 January 2005 in Bani et al. (2012). Note that, in the fourth grid, the two Marum and Benbow cones do not lie in the same grid box. As a result, we prescribed 60 % of the emission in the model grid box containing Marum and 40 % in the grid box containing Benbow as found in Bani et al. (2009). Note, that in the AEROCOM database, the value is $0.0807\,kt\,day^{-1}$. [d] Lopévi is a volcano with frequent degassing. According to Bani et al. (2006), vapor was observed covering the crater, but it was difficult to draw conclusions regarding its volcanic activity. Local observers in Vanuatu indicated ongoing eruptive activity at Lopévi starting at the end of January 2005 and continuing into February (GVP). As a result, we kept the value of AEROCOM database of $0.070\,kt\,day^{-1}$. [e] No information. Post-eruptive degassing rate of $0.070\,kt\,day^{-1}$ is assigned in the AEROCOM database. [f] Value of 10 January 2005 from Bani et al. (2012). In the AEROCOM database, it is $0.900\,kt\,day^{-1}$.

brym Volcano plume. We assumed that the aerosols size follows a lognormal distribution with a fixed median diameter ($D_{median} = 0.5\,\mu m$) and a fixed geometric standard deviation ($\sigma = 1.8$). On this basis, the number of aerosol particles was deduced from V_{aer}, D_{median} and σ, and the total aerosol surface densities ($cm^2\,cm^{-3}$) were then calculated (further details on lognormal aerosol distributions can be found in Seinfeld and Pandis, 2006). Here, the resulting surface area distribution (Fig. S4 in the Supplement) has a surface median diameter of 1 µm and a maximum surface area of $7000\,\mu m^2\,cm^{-3}$ in the near-downwind plume. This maximum value corresponds to a surface of $7 \times 10^{-11}\,\mu m^2$/molec SO_2^{-1}, a value that lies in the range of the order (10^{-11}–$10^{-10}\,\mu m^2$/molec SO_2^{-1}) studied by Roberts et al. (2014a). It is also broadly consistent with a recent estimate of aerosol surface area (relative to SO_2) made for Mt Etna (Vignelles et al., 2016). Ongoing developments are being made to improve the volcanic aerosol representation to include two modes with a diameter varying with hygroscopy, based on recent observations (Vignelles et al., 2016).

2.3.3 Emissions

To generate the emissions, we have used the preprocessor PREP_CHEM_SRC (version 4.3) code described in detailed in Freitas et al. (2011). Anthropogenic emissions were prescribed using the RETRO (REanalysis of the TROposhperic chemical composition) global database (Schultz et al., 2007). Fire emissions were estimated using the Global Fire Emissions Database (GFEDv2) with $1° \times 1°$ spatial resolution and an 8-day temporal resolution (van der Werf et al., 2006). Biogenic emissions were provided by a monthly mean climatology for the year 2000 produced with the MEGAN (Model of Emissions of Gases and Aerosols from Nature) database (Guenther et al., 2006). Details on the treatment of volcanic emissions and its modification for this study are given in the following.

SO_2 emissions

In CCATT-BRAMS, volcanic SO_2 emission rates are prescribed using the AEROCOM (Aerosol Comparisons between Observation and Models) database (Diehl et al., 2012; Freitas et al., 2011). This database includes volcanoes listed in the Smithsonian Institution's Global Volcanism Program database (GVP) (Siebert et al., 2010). Their emissions rates are assigned depending on their eruptive state (pre-eruptive, intra-eruptive, post-eruptive and extra-eruptive degassing), on their Volcanic Explosive Index (VEI) in case of eruption and on additional information from TOMS (Total Ozone Mapping Spectrometer), OMI instruments and COSPEC (correlation spectrometer) measurements) when available (Diehl et al., 2012).

Here, we replaced the values from the AEROCOM database for volcanoes of the Vanuatu Arc by more relevant information, when they were available. In particular, the SO_2 emission rate for Ambrym ($18.8\,kt\,day^{-1}$) is reported by Bani et al. (2009, 2012), using DOAS measurements (described in Sect. 2.2.1) in conjunction with wind-speed estimates. The error on this source is about ±20 % according to Bani et al. (2009).

SO_2 emissions rates of the most important volcanoes of the Vanuatu Arc in January 2005 are summarized in Table 2. Note that the Bagana Volcano (6.140° S, 155.195° E, alt = 1750 m) in Papua New Guinea was also active for the period of the simulation, with an emission of 3.3 kt day^{-1} of SO_2 according to the AEROCOM database.

HBr and HCl emissions

HBr and HCl emission rates are derived from the measurements of HBr, HCl and SO_2 average fluxes reported for Ambrym by Allard et al. (2009). These average fluxes were based on airborne DOAS (to determine SO_2 flux) combined with gas ratios (to SO_2) calculated from crater-rim deployments of filter-pack samplers (for HBr, HCl, HF with SO_2) and multi-gas sensors (for CO_2, H_2O with SO_2) and are representative of the mean volcanic emission of Ambrym (Allard et al., 2015). We did not use directly the HBr and HCl measurements but instead derived the HBr / SO_2 and HCl / SO_2 mass ratios (8.75×10^{-4} and 0.1, respectively) from the reported fluxes and applied them to our January 2005 SO_2 emission rate value to estimate the HBr and HCl emissions specifically for this date. Indeed, volcanic emission fluxes can vary with time. Allard et al. (2009) reported that the mean SO_2 emission rate for instance totals 8.8 kt day^{-1}, about 2 times smaller than the SO_2 emission rate reported during the extreme passive degassing event of 18.8 kt day^{-1} but in closer agreement with the estimate by Bani et al. (2012) of Ambrym mean activity of 5.4 kt day^{-1} for the period 2004–2009. The calculation yields HCl and HBr emissions of 1.9 kt day^{-1} and 16.5 t day^{-1}. It is of note that the HBr / SO_2 and HCl / SO_2 mass ratios are close to (for HBr / SO_2 perhaps somewhat higher than) mean estimates for volcanic degassing as reported by Pyle and Mather (2009), but due to the high Ambrym SO_2 flux they yield very high volcanic halogen fluxes. By comparison, the Br flux from Mt Etna is reported as only 0.7 kt year^{-1} (Aiuppa et al., 2005), i.e., 1.9 t day^{-1}, almost 10 times smaller. Note also that HF emissions were not considered in this study: whilst deposition impacts from HF around Ambrym can be severe (Allibone et al., 2010), HF does not contribute to reactive halogen cycling in the atmosphere (prevented by the strong H–F bond).

Sulfate emissions

We assume that 1 % of the sulfur (= $SO_2 + H_2SO_4$ here) is emitted as H_2SO_4 aerosol based on reported observations from several filter-pack studies at different volcanoes worldwide (e.g., Mather et al., 2003; von Glasow et al., 2009, and references therein).

Table 3. Composition inputs to the HSC Chemistry model assuming a plume–air mixture of 98 : 2 magmatic : atmospheric gases, with temperatures of 1125 and 20 °C, resulting in a mixed temperature of 1103 °C. Resulting output of the HSC Chemistry simulations were converted to ratios relative to sulfur and used to initialize the S1_HighT model simulation (second row of Table 4). The HSC Chemistry model is presented in Sect. 2.3.3

Gas	Mass mixing ratio in HSC input
H_2O	9.29×10^{-1}
N_2	1.56×10^{-2}
CO_2	3.80×10^{-2}
SO_2	1.05×10^{-2}
HCl	1.84×10^{-3}
O_2	4.20×10^{-3}
Ar	2.00×10^{-4}
HBr	7.23×10^{-6}
HF	7.53×10^{-4}

Initialization with output from HSC Chemistry thermodynamic model

As mentioned earlier (see Sect. 1), the mixing of volcanic gas with ambient air at the vent leads to high-temperature oxidative dissociation processes and hence to the formation of radical species. To take into account this high-temperature chemistry, the thermodynamic model HSC Chemistry (Roine, 2007) was applied to simulate the equilibrium chemical composition of the volcanic gas–air mixture, assuming a 98 : 2 volcanic gas : atmospheric gas composition. This approach follows that of previous 1-D model studies (Bobrowski et al., 2007; Roberts et al., 2009, 2014a; von Glasow, 2010; Kelly et al., 2013; Surl et al., 2015). The model temperature was based on mixing an atmospheric temperature of 20 °C (consistent with that predicted by the CCATT-BRAMS model) and the magmatic degassing temperature of 1125 °C estimated by Sheehan and Barclay (2016). This was based on the calculation of crystallization temperatures of mineral phases in scoria samples collected from Ambrym in 2005, following models of Putirka (2008). The HSC Chemistry model input composition, shown in Table 3, is a 98 : 2 mixture of magmatic gases (with composition based on Allard et al., 2009) and atmospheric gases (78 % N_2, 21 % O_2, 1 % Ar). Roberts et al. (2014a) identifies key new species in the HSC Chemistry output as Br, Cl, OH and NO. Fluxes of these species were calculated from their ratio to sulfur in the HSC Chemistry output and by scaling with the (prescribed) SO_2 flux in the CCATT-BRAMS model. Due to uncertainty in volcanic NO_x emissions (see discussions of Martin et al., 2012; Roberts et al., 2014a; Surl et al., 2015), HSC Chemistry outputs both with and without NO_x were used to initialize CCATT-BRAMS (Simulations S1_HighT and S1_HighT_noNOx). Note that the HSC output also contains SO_3, which is the

Table 4. Emissions of HCl, HBr, sulfate and radicals (Cl, Br, OH, NO) expressed in terms of mass ratios relative to SO_2 emissions for all the volcanoes within the domain study and for the different simulations (see Sect. 2.3.3 for the details on the ratio derivation and Sect. 2.3.4 for details on the simulations). Note that for S1_no_hal, S1_no_hal2 and S0 simulations, the ratios indicated here are only for the emissions of Ambrym Volcano. These simulations have the same emissions as S1_HighT for the other volcanoes within the domain study. Note also that all the simulations, except S0, have an SO_2 emission for Ambrym of 18.8 kt day^{-1}. S0 does not include any volcanic emissions from Ambrym.

Simulations	HCl / SO_2	HBr / SO_2	H_2SO_4 / SO_2	Cl / SO_2	Br / SO_2	OH / SO_2	NO / SO_2
S1	0.1	8.75×10^{-4}	1.55×10^{-2}	0	0	0	0
S1_HighT	0.1	6.87×10^{-4}	1.55×10^{-2}	1.33×10^{-4}	1.89×10^{-4}	7.04×10^{-4}	7.45×10^{-4}
S1_HighT_noNOx	0.1	6.87×10^{-4}	1.55×10^{-2}	1.33×10^{-4}	1.89×10^{-4}	7.04×10^{-4}	0
S1_no_hal Ambrym only	0	0	0	0	0	0	0
S1_no_hal2 Ambrym only	0	0	0	0	0	7.04×10^{-4}	0
S0 Ambrym only	0	0	0	0	0	0	0

precursor to volcanic sulfate. However, as mentioned above, in this study the volcanic sulfate emission was instead fixed to 1 % (by mole) of sulfur in all runs. All the emissions for the different simulations are summarized in Table 4.

Plume height

The information on plume heights is from the AEROCOM database and from Bani et al. (2012). They give, respectively, plume heights of 1373 and of 2000 m (in our study, all the altitudes are above sea level unless otherwise mentioned). Note that the mean altitude of both crater rims is about 1000 m. Bani et al. (2012) report an altitude of the plume of 2000 m for the degassing event of 12 January 2005 that was estimated visually. For the other periods, their estimation of the altitude varies between 700 m (i.e., below the craters) and 2000 m. For the case study of the degassing event of January 2005, it was not clear to us from videos and pictures that the plume altitude was about 2000 m. As a result, we performed a sensitivity study on the plume height (see Supplement). In a first simulation, emissions are injected in the model box vertically above the volcano that includes the 1373 m altitude point. This model box is not the same in each grid, as the topography depends on the grid resolution. As a result, its depth varies between about 100 and 200 m. In a second simulation, emissions are injected higher up in the box containing the 2000 m altitude, whose depth varies between about 200 and 300 m. As shown later, we performed an additional sensitivity analysis, where the emissions are this time spread over two vertically adjacent grid boxes (Sect. 3.3.1). The depth of the plume in the model this time is about 300 to 400 m. Figure 1 shows the distribution of volcanic emissions in the vertical prescribed in the model for the different sensitivity simulations.

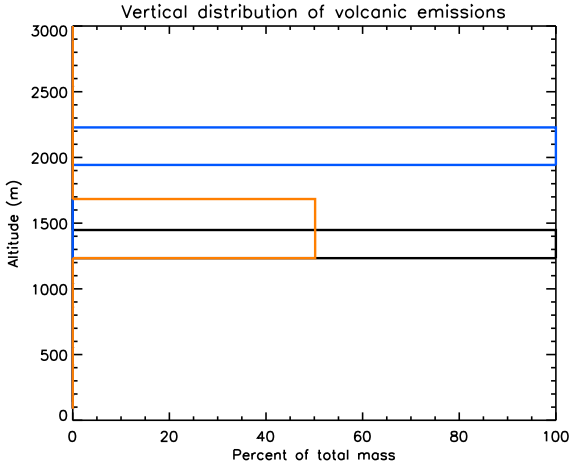

Figure 1. Vertical distribution of volcanic emissions from Ambrym as prescribed in the model for the all the simulations (black line) except for the sensitivity simulations S1_HighT_alt (blue line) and S1_HighT_width (orange line). See Sect. 2.3.4 for details on simulations.

2.3.4 Model general setup and simulations

In our study, the primary horizontal resolution is 50 km × 50 km with 44 vertical levels from the ground to 27 km. Three nested grids (10 km × 10 km, 2 km × 2 km and 0.5 km × 0.5 km) were also added. Model domain and grids are shown in Fig. 2. Horizontal winds, geopotential height, air temperature and water vapor mixing ratios from ECMWF analysis (with a 0.5° × 0.5° resolution) are used to initialize and nudge the model using a four-dimensional data assimilation (4DDA) technique with a relaxation time constant ranging from 30 min at the lateral boundaries to 6 h at the center of the domain. Initial and boundary conditions for concentrations of the chemical species were provided by 6-hourly output from the global chemical transport model MOCAGE (Josse et al., 2004) with a resolution of 1° × 1°.

In the following, we describe the different simulations performed in this study. All the simulations start on the 1 January 2005 at 00:00 UTC with the larger grid only. As this was an extreme degassing event of long duration (several months) rather than an episodic eruption, the model initial-

ization from 1 January 2005 already includes the Ambrym emissions. Due to computing limitations, the three nested grids are only added the 11 January 2005 00:00 UTC, with the initial conditions given by the corresponding simulation with one grid. The different simulations differ in terms of the strength of the emissions, the nature of the emitted compounds and the repartition of the emissions in the vertical. They are summarized below, as well as in Table 4 and Fig. 1:

- S1 includes the standard volcanic emissions (SO_2, H_2SO_4, HCl, HBr).
- S1_HighT includes emissions (SO_2, H_2SO_4, HCl, HBr, OH, NO, Cl, Br) derived from an HSC Chemistry simulation described in Sect. 2.3.3 and in Table 3.
- S0 has the same emissions as S1_HighT except that emissions from Ambrym Volcano have been turned off.
- The S1_HighT_alt simulation is exactly the same as S1_HighT except that the height of the plume is fixed to 2000 m.
- S1_HighT_width is exactly the same as S1_HighT except that the plume of Ambrym spans two grid boxes (in the vertical) instead of one.
- The S1_HighT_noNOx simulation is exactly the same as S1_HighT except that emissions of NO have been turned off.
- S1_nohal has the same emissions as S1_HighT except that Ambrym Volcano includes only SO_2 emissions.
- S1_nohal2 has the same emissions as S1_HighT except that Ambrym Volcano includes only SO_2 emissions and the same emissions of OH than S1_HighT.
- S1_HighT_surf is exactly the same as S1_HighT except that area surface density was increased by a factor of 10.

In the next section, we evaluate the performances of the model CCATT-BRAMS to simulate near-downwind volcanic plume chemistry for the Ambrym extreme passive degassing of 12 January 2005 using the airborne DOAS observations of SO_2 and BrO columns in the context of previous work.

3 Analysis of the modeled volcanic chemistry in the near-downwind plume

3.1 Evaluation of the modeled SO_2 and BrO columns amounts in the near-downwind plume

Figure 3 shows the SO_2 columns amounts observed during four traverses of the near-downwind Ambrym plume (between 15 and 40 km of the vent) on 12 January 2005 between 05:00 and 06:00 UTC (Bani et al., 2009, 2012) and the corresponding SO_2 columns amounts simulated by the model for

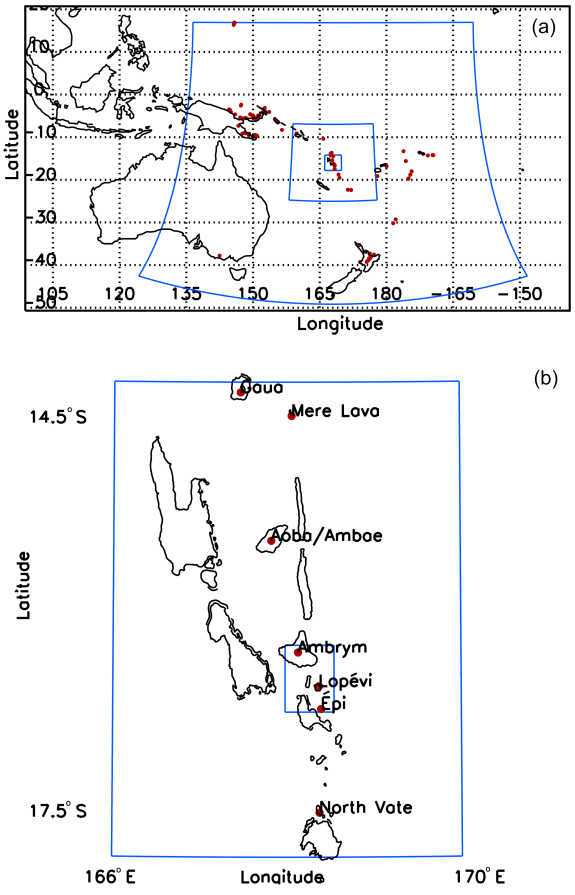

Figure 2. (a) Position of the nested model grids (blue lines) and of the volcanoes (red filled circles) taken into account in the simulations. For clarity, only the three largest model grids are shown. **(b)** Zoom on the two smallest model grids (blue lines) and on the volcanoes (red filled circles) taken into account in the simulations. Resolution of each grid is given in Sect. 2.3.4.

the S1 (i.e., including the standard emission) and S1_HighT (i.e., initialized with the output of the HSC Chemistry model as described in Sect. 2.3.3) on the 0.5 km × 0.5 km grid (see Sect. 2.3.4 for the description of the simulations). Statistical quantities (mean, RMS, correlation) were calculated to compare observations and simulations more quantitatively (Table 5). Note that sensitivity studies to the height of the plume and the vertical extent of the plume will be discussed further in Sect. 3.3.

3.1.1 SO_2 columns

Observations show that SO_2 columns decrease with distance from the vent and exhibit a bimodal distribution across the plume. Each mode is attributed by Bani et al. (2009) to the individual plume of the two degassing craters Benbow and Marum, which are situated 3 km apart. Figure 3 shows that the model captures the magnitude of the SO_2 columns relatively well along and across the plume for the S1 and

Table 5. Statistical comparison between the DOAS SO_2 and BrO columns from the five traverses of the Ambrym plume on 12 January 2005 and the corresponding simulated values (for S1 and S1_HighT). Correlation coefficients (r), root mean square error (RMSE in molecule cm^{-2}) are given as well as mean values (molecule cm^{-2}) of observed and simulated data. Note that we did not include the data here for which we did not have GPS data (dashed lines of Figs. 3 and 4).

	Mean SO_2	Mean BrO	r_{SO_2}	r_{BrO}	$RMSE_{SO_2}$	$RMSE_{BrO}$
DOAS	2.29×10^{18}	5.84×10^{14}				
S1	2.27×10^{18}	1.14×10^{14}	0.62	−0.21	1.09×10^{18}	5.97×10^{14}
S1_HighT	2.25×10^{18}	3.42×10^{14}	0.61	0.59	1.10×10^{18}	3.90×10^{14}

S1_HighT simulations. The mean difference between observations and simulations is lower than 2 % (relative to the mean of the observation) and the correlation coefficient is about 0.6 (Table 5). However, we note that the influence of the two craters Benbow and Marum is not seen as clearly as in the observations. This suggests a limitation linked to the model resolution, even though the model resolution for the particular grid shown is 500 m × 500 m. We can also note that the simulated plume tends to be slightly tilted eastward compared to the observations, in particular for the transects at 20 and 21 km (not shown) from the vent and to a lesser extent for the transect at 40 km. This is the reason for the relatively high RMS values (about 50 % of the mean SO_2, see Table 5), but it does not affect the bias (2 %).

Previous work at volcanoes elsewhere (e.g., Bobrowski et al., 2007) reported that the observed SO_2 variations in the near-downwind plume are almost exclusively due to plume dilution. As a test, we have included in our simulation an SO_2 "tracer" whose emission and deposition are the same as for SO_2 but whose chemical loss is equal to zero. We find that the difference between the SO_2 columns field and the SO_2 tracer columns field at a distance of 40 km from the vent is less than 0.5 % (not shown), confirming that the SO_2 decrease in the model with distance from the vent in Fig. 3 is mostly due to plume dilution. Therefore, we can conclude from the comparison in Fig. 3 that the direction of the plume as well as its dilution are reasonably well simulated by the model in the simulations S1 and S1_HighT. It is important to note that we cannot conclude here on the strength of the Ambrym SO_2 source. Indeed, our reasoning would be circular as, in our model, we have used the SO_2 source strength (described in Sect. 2.3.3 and Table 2) which Bani et al. (2009, 2012) derived from the same DOAS data (combined with wind estimates) used here for the model evaluation. Note also that we performed a simulation S1_HighT_alt, similar to S1_HighT except that the plume height was 2000 m as reported by Bani et al. (2012). We find that the simulation S1_HighT_alt (see Supplement, Sect. S1 as well as Figs. S1 and S2 for more detail) underestimates the observations by 44 % for SO_2 (compared to 2 % for S1_HighT). The correlation between simulated and observed SO_2 is also reduced: 0.37 compared to 0.61 for S1_HighT. Given better agreement between the model and observations at the lower injection altitude estimate of ∼ 1400 m, this injection height of S1_HighT was used in the following.

3.1.2 BrO columns

In Fig. 4, the same comparison as for Fig. 3 is presented for BrO columns amounts. BrO columns, as those of SO_2, decline between 15 and 40 km from a mean of 9.8×10^{14} to a mean 3.2×10^{14} molecule cm^{-2}. Values as high as 1.8×10^{15} molecule cm^{-2} at 15 km were reported by Bani et al. (2009). Note that these values are particularly high compared to other BrO column observations at volcanoes elsewhere, for which maximal values lie between 10^{14} and 10^{15} molecule cm^{-2} (Boichu et al., 2011). Note also that the influences of the two crater sources (Benbow and Marum) are still visible in the BrO data as two distinct peaks.

In the standard simulation, the trend in BrO with distance from the vent is reversed compared to the observations (also shown by the negative correlation coefficient of Table 5 of −0.21). At 15–20 km downwind from the vents, where observed BrO columns are highest, the model (S1) underestimates the mean BrO columns by a factor of 10. Overall, the mean difference between BrO columns observed and those simulated in S1 is about 80 % (Table 5). For the simulation initialized with the HSC Chemistry model, the trend in BrO with distance from the crater is in better agreement with the observations (Fig. 4 and correlation coefficient of Table 5 of 0.6). An improved overall agreement between model and observations is also found (as seen in Fig. 4 and Table 5): the mean bias between observed and simulated BrO columns is about 40 % (relative to the mean observations). It is important to note that the bias is more pronounced near the source: it varies from 60 % for the transect at 15 km to 14 % for the one at 40 km of the vents.

Figure 5 shows the evolution of BrO / SO_2 with distance from the vent derived from the observations and from the simulations presented in Figs. 3 and 4. Because SO_2 can be considered a passive tracer on short timescales, any increase or decrease in BrO / SO_2 implies, respectively, a production or a destruction of BrO. Measurements suggest that BrO formation has occurred and has reached its maximal amount between 0 and 17 km of the vent. Further downwind, between 17 and 40 km, measurements predict a destruction of BrO. In the simulation initialized with the HSC Chemistry model,

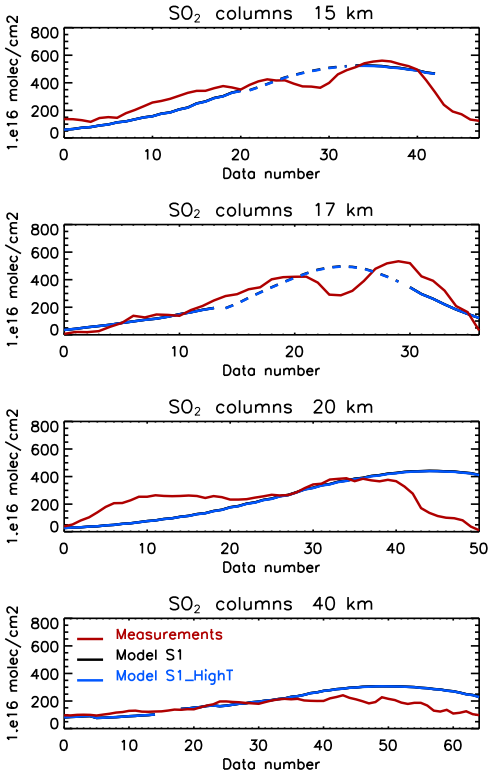

Figure 3. Comparison between SO_2 columns observed by Bani et al. (2009) (red line) and simulated by the model for S1 (black line) and S1_HighT (blue line). Each panel represents a traverse of the Ambrym plume in the crosswind direction on the 12 January 2005 between 05:00 and 06:00 UTC, at a range of distances downwind. The traverse at 21 km from the source is not shown here but is included in Table 5. The x axis shows the data point number in the transect across the plume (Bani et al., 2009). The direction of each transect across the plume has an east–west component. Here, each transect is shown with the data points from west to east (left to right). Note that model results are for the same position and time as the measurements and for the finest grid (0.5 km × 0.5 km) except when GPS data (longitude and latitude) were not available. In this case, model results (dashed lines) were interpolated between the last and the next positions for which we had GPS data. Note that black and blue lines are on top of each other (superimposed). Reported error from DOAS measurements (1σ) is 2.45×10^{16} molec cm^{-2}.

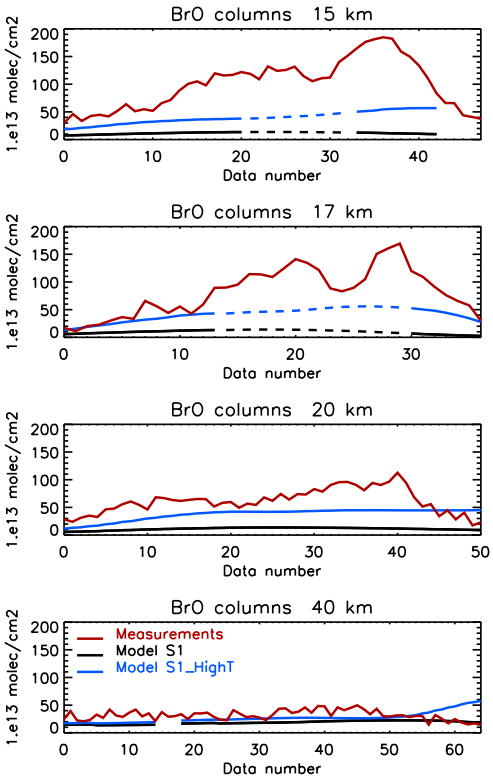

Figure 4. Comparison between BrO columns observed by Bani et al. (2009) (red line) and simulated by the model for S1 (black line) and S1_HighT (blue line). See Fig. 3 for details on the method of comparison. Reported error (1σ) is 1.22×10^{14} molec cm^{-2}.

the trend in BrO / SO_2 is close to that observed. The formation of BrO reaches a maximum around 17 km with a plateau between 17 and 21 km, and BrO is destroyed between 20–21 and 40 km. In contrast, in the case of the standard simulation S1, BrO builds up between 15 and 40 km. Overall, we conclude that BrO formation is too slow in the standard simulation compared to the observations. In contrast, the kinetics of BrO formation predicted in the simulation initialized with HSC Chemistry model is in good agreement with the observations. This confirms previous 1-D model work that showed the need for radicals to "kick off" the chemistry, i.e., accelerate the onset of the chemistry (e.g., Bobrowski et al., 2007; Roberts et al., 2009). In addition, Fig. 5 shows that, for each transect, the variability of BrO / SO_2 ratios in the observations and in the S1_HighT simulation has a similar magnitude. In particular, we find that for each transect the model simulates the highest value of the BrO / SO_2 ratio at the edges of the plume as shown in the observations, i.e., for the lowest values of SO_2 columns. This result is again consistent with previous work (e.g., Bobrowski et al., 2007; von Glasow et al., 2009; von Glasow, 2010; Roberts et al., 2014a). At the edges of the plume, more mixing with entrained background air occurs. This leads to higher ozone concentrations and favors BrO (see Sect. 2.1.2). In general, the trends in BrO / SO_2 with distance downwind and between the core and plume edge reflect the net impact of a dynamic chemistry involving many reactive bromine chemistry species. In the following section, we analyze in more detail the simulation of volcanic plume chemistry.

3.2 Simulated plume chemistry

Figure 6 shows distance–pressure cross sections of SO_2, OH, HBr, BrO, O_3 and NO_x mixing ratios in the plume of the standard simulation for the 12 January 2005 at 06:00 UTC

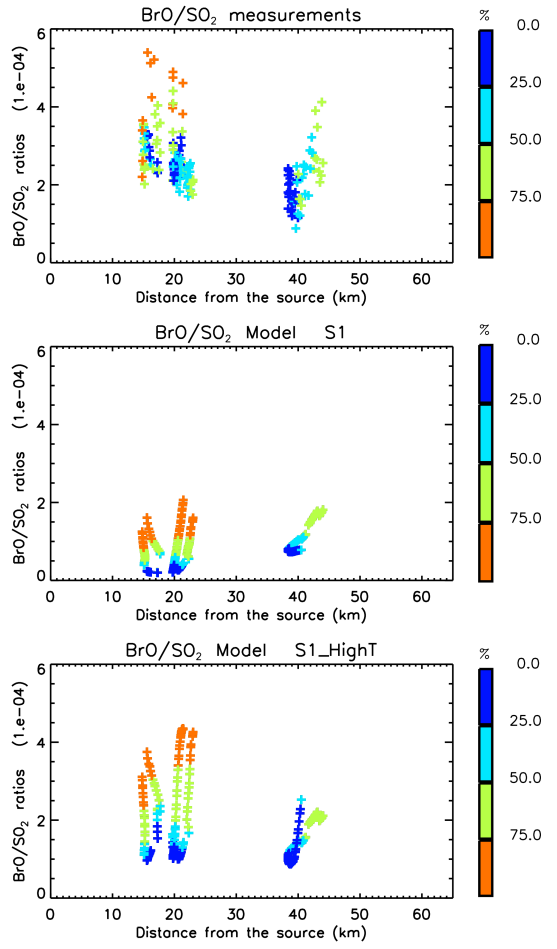

Figure 5. Variation of BrO / SO_2 ratios with distance from the vent derived from observations (top) and model simulations S1 (middle); S1_HighT (bottom) presented in Figs. 3 and 4. For each transect, each BrO / SO_2 ratio has been colored according to its SO_2 column value relative to the maximal value of the SO_2 column (SO2_max) for this transect. More precisely, the color indicates the relative difference $\frac{(SO2\_max - SO2)}{SO2\_max}$. Note that we did not include the observations nor the corresponding model results for which we did not have GPS data (dashed lines of Figs. 3 and 4).

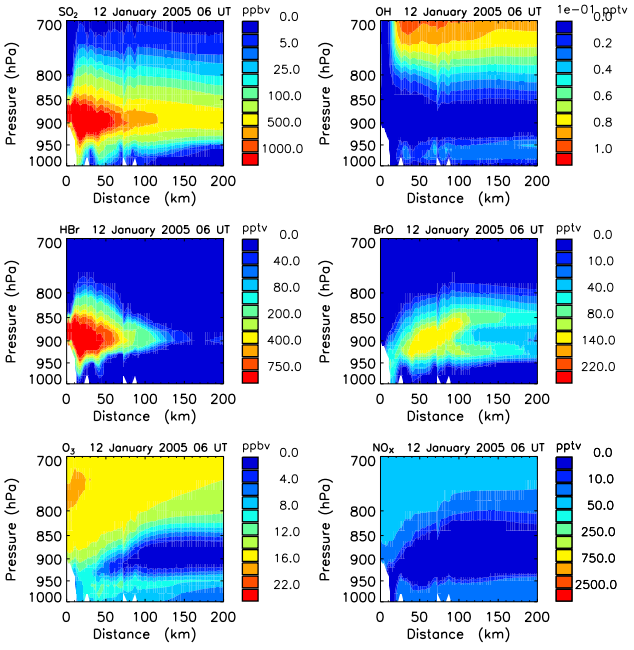

Figure 6. Distance–pressure cross section of the SO_2, OH, HBr, BrO, O_3 and NO_x mixing ratios in the plume of Ambrym on 12 January 2005 at 06:00 UTC in the simulation S1.

(time of the DOAS measurements) in the 2 km × 2 km grid. This grid allows us to visualize the results as far as 200 km downwind. Figure 7 shows the Br speciation among the bromine species along the plume (in the core and at the edges) for the same simulation on the same grid and at the same time. Figure 6 shows that OH is totally depleted in the core of the plume in the simulation. This is due to the elevated concentrations of SO_2 as well as being a consequence of the halogen chemistry (see Sect. 4.4) and mirrors findings from previous 1-D model studies (e.g., Roberts et al., 2009, 2014a; von Glasow, 2010). However, as noted before, the decrease in SO_2 along the plume as far as 200 km is mainly due to the dilution of the plume. Figures 6 and 7 show that HBr is converted into reactive bromine in the volcanic plume, as expected. However, at about 50 km from the vent, only 20 % of this conversion had occurred (80 % HBr remains). Indeed, the chemical cycle responsible for HBr conversion is autocalytic, so it needs reactive bromine to be initiated. In the standard simulation, the onset of BrO formation is slow because reactive bromine is initially formed by the reaction of HBr with OH, which is slow because OH is depleted. In Fig. 6, the enhancement of BrO (and of Br_2 in Fig. 7) as well as the depletion of O_3, NO_x and HO_x (not shown) confirm that the autocatalytic cycle responsible for HBr conversion to reactive bromine is ongoing in the simulations (see Sect. 2.1.2). Very quickly, in the core of the plume, BrO becomes the dominant species after HBr. Its mixing ratio increases with distance from the vent, reaching a maximum of 120 pptv at about 70 km (Fig. 6), equivalent to 20 % of the total bromine (Fig. 7). The depletion of ozone reaches its maximum of a loss of 15 ppbv (100 %) at 70 km, corresponding to the maximum of BrO. Further downwind, Br is the dominant species because O_3, HO_x and NO_x are depleted. In contrast, at the edges of the plume, BrO is still increasing and dominates because more ozone is available than in the core of the plume, enabling its formation from Br (Reaction R3). Further downwind at the edges of the plume, the formation of BrO slows but does not stop (as shown by the nonzero Br_2 and BrCl fraction) as the plume disperses and dilutes the volcanic aerosol. A dynamic equilibrium is established between BrO, Br and HOBr. We note that the BrO mixing ratio remains as high as 60 pptv at the edge of plume around 200 km downwind (Fig. 6).

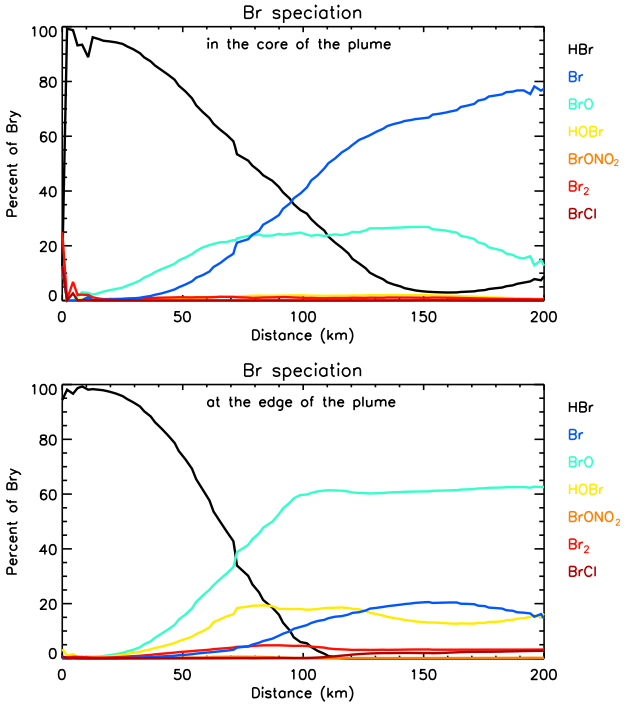

Figure 7. Br speciation along the plume (in the core and at the edge) in the simulation S1 and the 2 km × 2 km grid for the 12 January 2005 at 06:00 UTC. The Br speciation has been calculated as the percent of Br_y ($Br_y = HBr + 2Br_2 + BrCl + Br + BrO + HOBr + BrONO_2$). Distance is calculated from the middle of the grid box containing Marum and Benbow.

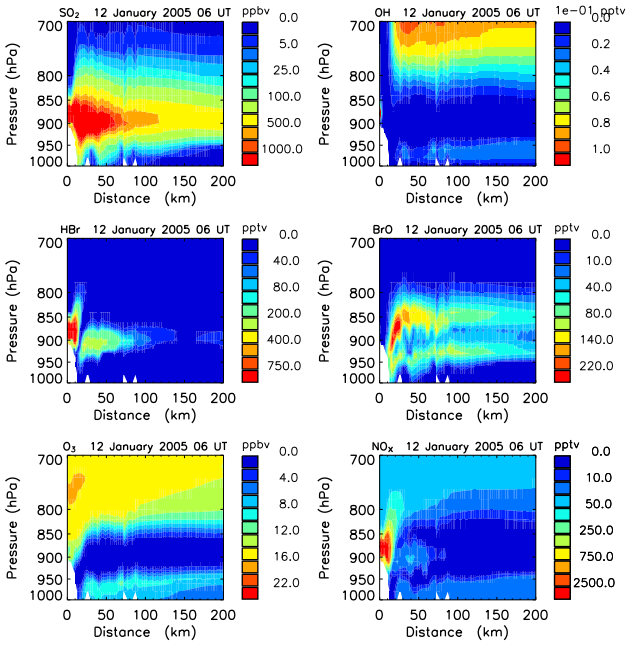

Figure 8. Distance–pressure cross section of the SO_2, OH, HBr, BrO, O_3 and NO_x mixing ratios in the plume of Ambrym on 12 January 2005 at 06:00 UTC in the simulation S1_HighT.

As expected, in the simulation initialized with the HSC Chemistry model, the conversion of HBr into reactive bromine is accelerated by the presence of the radical species (Figs. 8 and 9). Indeed, the HBr fraction is only 20 % at 25 km from the vent and is almost zero around 30 km downwind at the edge of the plume. Once HBr becomes depleted, a peak of BrCl is observed because the aqueous phase equilibria between BrCl and Br_2 favor BrCl instead of Br_2. Figure 8 shows that BrO reaches its maximum earlier, around 15–20 km downwind, than for the standard simulation (70 km), at a distance where the plume is more concentrated. As a result, the maximum of BrO mixing ratios is higher (around 240–260 pptv) than for the standard simulation. Ozone is also entirely depleted in this simulation, it reaches a loss of 15 ppbv (100 %) around 15 km. In the core of the downwind plume, Br becomes the dominant species (up to 80 % of Br_y; Fig. 9) due to this total ozone depletion with ongoing ozone loss processes exceeding any source from the entrainment of (ozone-containing) background air into the plume core. HBr can re-form by the reaction of Br with HCHO, for instance, because of the high concentrations of Br in the core of the plume. Further downwind, HBr is then reconverted into BrO, likely because a somewhat enhanced entrainment of ambient air occurs. At the edges of the plume, the chemical cycles are not limited by the lack of (background) oxidants. As a result, HBr can be fully consumed and BrO is the dominant species. Further downwind, the formation of ongoing reactive halogen chemistry results in a dynamic equilibrium being established between BrO, Br and HOBr. We also note that even further downwind (approximately 150 km from the vent), there is no significant difference between S1 and S1_HighT in terms of the absolute concentration of the bromine species and in terms of partitioning among the bromine species.

To conclude, the kinetics of BrO formation predicted in the simulation initialized with the HSC Chemistry model is in good agreement with the observations. This leads to higher BrO concentrations in the near-downwind plume and hence to a better comparison with DOAS data. Despite the better comparison between DOAS and S1_HighT, the model still underestimates the BrO columns in the near-source plume by 60 % (at 15 km from the vents). We find that this is due to the ozone depletion in the core of the plume that limits the formation of BrO from Br. In strong (i.e., near-source and high-emission) volcanic plumes, gas-phase cycling between Br and BrO (Reactions R3, R4a and R4b) is particularly intense. As a consequence, in the core of the plume where the mixing with background ozone is limited, ozone is totally depleted. This lack of ozone limits the partitioning of BrO from Br and hence BrO concentrations.

As presented in Sect. 2.3, we had to make some assumptions in our study because of the lack of information to constrain the model or technical limitations. In the next section, we test whether the uncertainties in the representation

of some of the crucial processes could affect the model results and explain the discrepancies found between simulations and observations for the closest transects (∼ 15–20 km) from the vents. More specifically, we focus on the depth of the plume that controls the degree of mixing between emissions and background air, the formation of NO_x by the high-temperature chemistry and the surface aerosol area that can affect the in-plume chemistry.

3.3 Sensitivity studies

3.3.1 Vertical depth of the plume

A suggested in Sect. 3.2, BrO formation appears to be limited by ozone concentrations in the simulation S1_HighT. However, values of background ozone in the model seem in good agreement with ozone climatology (e.g., Logan, 1999), which indicates ozone mixing ratios of 15–20 ppbv below 800 hPa in the Pacific region. Here, in an attempt to avoid the limitation on BrO formation due to a lack of ozone, we have increased the degree of the mixing between the emissions and the background air in the vertical. Practically, we have artificially increased the vertical depth of the plume by spreading out the emissions over two vertically adjacent levels (see Fig. 1). More specifically, in the simulation S1_HighT_width, the emissions were distributed equally between the vertical grid box of the S1_HighT simulation and the one just above. As a result, the Br molecules are exposed to roughly twice as many ozone molecules. Note that we did not change the degree of mixing in the horizontal because Fig. 3, showing the comparison of SO_2 column distribution across the plume, seems to indicate that the width of the plume at different distances from the vents is reasonably well simulated by the model.

We find that the comparison with DOAS for SO_2 does not improve (mean bias of 17 % and a correlation of 0.55; Fig. S1). Concerning BrO, our results are very similar to those obtained with S1_HighT (slightly worse with a mean bias of 43 % and with a correlation coefficient of 0.54; Fig. S2). The weak impact of this sensitivity study can be explained by the fact that the vertical diffusion in the model has already dispersed the emissions very quickly through several vertical levels in S1_HighT. Thus, BrO formation is already limited by ozone in the upper level where the emission was additionally injected into S1_HighT_width. As a result, we have tried different combinations to spread out the emissions over more than 2 levels in the vertical between the level of injection of S1_HighT (∼ 1400 m) and the level of injection of S1_HighT_alt (∼ 2000 m) (see Fig. 1). But the wind direction changes with the altitude between these two levels in our simulations. Therefore, the comparison of SO_2 column distribution across the plume, which was fairly good for S1_HighT, worsens in these model runs and tends to become very similar to the one obtained with S1_HighT_alt (see Fig. S1).

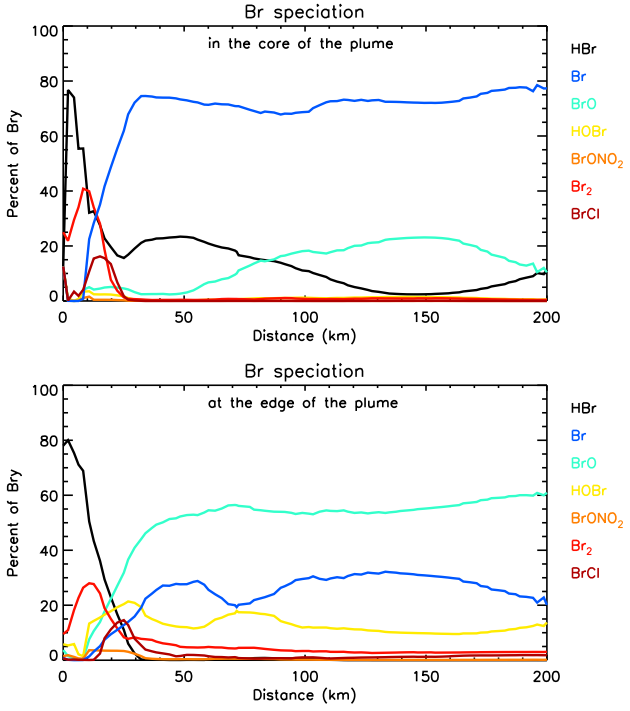

Figure 9. Br speciation along the plume (in the core and at the edge) in the simulation S1_HighT and the 2 km × 2 km grid for the 12 January 2005 at 06:00 UTC. The Br speciation has been calculated as the percent of Br_y ($Br_y = HBr + 2Br_2 + BrCl + Br + BrO + HOBr + BrONO_2$). Distance is calculated from the middle of the grid box containing Marum and Benbow.

3.3.2 Formation of NO_x by high-temperature chemistry

There are numerous uncertainties concerning the high-temperature chemistry taking place in the mixture of volcanic gases and ambient air at the vent (Martin et al., 2009, 2012). In particular, models used to calculate this chemistry assume thermodynamic equilibrium. However, Martin et al. (2012) calculated that the thermal N_2 fixation is too slow for equilibrium to be attained at volcanic vents. Hence, the production of NO_x by the HSC model could be overestimated. Conversely, volcanic NO_x production is suggested by several observations of NO, NO_2, HNO_3 and HO_2NO_2 in the near-source plume (e.g., Mather et al., 2004; Oppenheimer et al., 2010; Martin et al., 2012; Voigt et al., 2014), with an NO_x to HNO_3 conversion pathway proposed by Roberts et al. (2009, 2014a). In the case of Ambrym, no information is available on the absence or presence of volcanic NO_x or other reactive nitrogen species in the plume. We performed a simulation (S1_HighT_noNOx) where NO_x from the high-temperature initialization was not included while keeping the emissions of the other radicals constant (i.e., OH, Cl, Br) from HSC Chemistry. In this case, the SO_2 field is exactly

the same as in S1_HighT (Fig. S1). The comparison between BrO in S1_HighT_noNOx and the observations (Fig. S2) is very close to what is obtained for S1_HighT (mean model observation difference is about 44 % and the correlation is about 0.63). Figure S3 gives an explanation for this. It shows that the kinetics of HBr conversion in S1_HighT_noNOx is similar to that in S1_HighT in the first 10–15 km from the vent, and it is much slower after 15 km. This suggests that NO_x emissions are not crucial to kick off the plume chemistry initially but that they are responsible for the decline in HBr further downwind after 15 km. This delayed role of the NO_x radicals was also found in a 1-D model study presented by Roberts et al. (2009) (see their Fig. 4). In our case, this is further confirmed by Fig. 8, where it can be seen that NO_x depletion in S1_HighT starts after 10–15 km. The role of NO_x is linked to the formation of $BrONO_2$ from BrO and NO_2, followed by its rapid hydrolysis on volcanic sulfate aerosol that acts to convert BrO into HOBr and that can then undergo another heterogeneous chemical cycle to release reactive bromine from HBr ($Br^-_{(aq)}$). Without NO_x, this conversion of BrO into HOBr depends on the presence of HO_2 via the reaction of BrO with HO_2. Note also that due to the slower decrease in HBr in S1_HighT_noNOx after 10–15 km, no BrCl peak is visible in Fig. S3 in the near-downwind area in contrast to Fig. 9 for the S1_HighT simulation. To conclude, the difference in BrO kinetics in S1_HighT and S1_HighT_noNOx is mostly visible after 10–15 km from the vent. Hence, it does not impact the initial near-downwind rise in BrO. This contrasts with the model studies of von Glasow (2010) and Surl et al. (2015) for Mt Etna, who suggested that a volcanic NO_x emission acts to lower plume BrO due to the formation of $BrNO_2$ that persists in the plume. However, Roberts et al. (2014a) highlighted additional pathways for $BrNO_2$ removal enabling the regeneration of BrO. Given uncertainties in the chemistry, $BrNO_2$ is not included in our study.

To conclude, the simulations S1_HighT and S1_HighT_noNOx exhibit similar kinetics of BrO formation and also a similar magnitude in the BrO maximum. As a result, uncertainty in the presence of volcanic NO_x in the emission cannot explain the discrepancy between the model and reported downwind plume BrO. In addition, we also note that the BrO and SO_2 column measurements alone are not sufficient to fully constrain the parameter space of our modeling of volcanic plume chemistry. In particular, NO_x and HNO_3 / nitrate should be measured in volcanic plumes to constrain the reactive nitrogen emission.

3.3.3 Sulfate aerosol surface density

Despite a broad agreement with previous estimates (see Sect. 2.3.2), aerosol surface density remains a source of uncertainty in our study as we do not have direct measurements of aerosols for Ambrym. Therefore, we have increased the sulfate aerosol surface density by a factor 10, still keeping the value in the right range of order (Sect. 2.3.2), to test whether this uncertainty could explain the pronounced discrepancy in near-source BrO columns. We would expect that an increased aerosol surface area would increase the conversion of HBr into reactive bromine and hence the concentrations of BrO. Note, that this sensitivity study is equivalent to increasing the HOBr reactive uptake coefficient on sulfate aerosols, for which large uncertainties exist (see Roberts et al., 2014a), while keeping the aerosol surface area constant. We find that our sensitivity study only impacts the value of near-source BrO columns very slightly (bias of 62 % compared to the bias of 60 % for S1_HighT). Indeed, BrO is determined by the partitioning with Br mainly by Reactions (R3), (R4a) and (R4b) in the concentrated plume. Because ozone is quickly consumed, the formation of BrO is limited as discussed earlier. This is also in agreement with the sensitivity studies performed with the PlumeChem model (Roberts et al., 2014a) for Mt Etna, where increasing the aerosols surface density by a factor 10 only slightly increased the BrO / SO_2 ratio in the near-downwind plume. Note that we did not test the sensitivity of the model results to the strength of total bromine emissions. Increasing total bromine emissions would increase total bromine in the plume. But because of the ozone limitation, this would lead to a reduced fraction of BrO and an increased fraction of Br. Finally, these two effects would compensate each other, as found with a 1-D model for the Nyiragongo's plume by Bobrowski et al. (2015). As a result, increasing total bromine emissions would not impact BrO columns. This compensation was also found by Roberts et al. (2014a) with their 1-D model when they compared their "high" and "medium" total bromine scenarios.

To conclude, the uncertainties on plume depth, NO_x emissions, aerosol loading and injection height cannot explain the discrepancy between the model and the reported near-source BrO. Instead, we find that BrO formation is ozone limited in our model runs. This is also found in the model 1-D runs of Bobrowski et al. (2015) of the Nyiragongo's plume; they conclude that measurement of ozone should be a priority for the next measurement campaigns. More generally, BrO and SO_2 column measurements are not sufficient to constrain the modeling of volcanic plume chemistry as also highlighted in Bobrowski et al. (2015). It is also important to note that the discrepancy between simulated and measured BrO columns remains limited to the near-downwind plume. Indeed, the modeled BrO columns agree within 14 % with the farthest observations ($\sim$ 40 km from the vents). As the result, this discrepancy does not significantly impair the analysis of the regional impact of Ambrym presented below.

4 Regional impact of Ambrym volcanic emissions

4.1 Evaluation of the plume simulation on the regional scale with OMI

Figure 10 shows SO_2 columns on 12 January 2005 at 02:30 UTC from OMI and the corresponding SO_2 columns interpolated on the OMI grid from CCATT-BRAMS. The model result is for the grid resolution of 10 km × 10 km, is of a similar size to the OMI data (13 km × 24 km). At this time of the year, the plumes from Marum and Benbow are generally carried to the northwest by the trade winds. As shown in Fig. 10, on 12 January 2005, they were carried to the south because of the influence of the Cyclone Kerry, located around 1800 km southwest of Vanuatu (Bani et al., 2009). Figure 10 suggests that the direction of the plume is correctly simulated on the regional scale. To quantify the degree of spatial matching between modeled and observed SO_2 plumes, we have calculated the figure of merit in space (FMS), which is the intersection of the observed and simulated plume areas divided by the union (in the sense of set theory) of these areas (see Mosca et al., 1998, for more details). Using a threshold of 5×10^{16} molec SO_2 cm^{-2} to define the Ambrym plume in both OMI and model fields, we find an FMS of 62 % that suggests a fairly good spatial agreement between observed and modeled plumes. The difference between observed and simulated SO_2 columns distributions is mainly due to the plume width that is slightly larger in the simulations than in OMI data (Fig. 10). The magnitudes of the mean columns in both plumes also match fairly well: the mean difference is about 25 % (relative to the observations). This difference is due to the presence of some SO_2 enhancements in the plume in the OMI data that are not seen in the simulations. Note that the truncated length of the SO_2 plume in the OMI data is related to the presence of clouds northeast of New Caledonia. It is important to note that the present comparison also shows that simulated SO_2 columns, when initialized with the Ambrym SO_2 source strength estimate derived from the DOAS observations by Bani et al. (2009, 2012), agree within 25 % with the SO_2 columns detected by OMI.

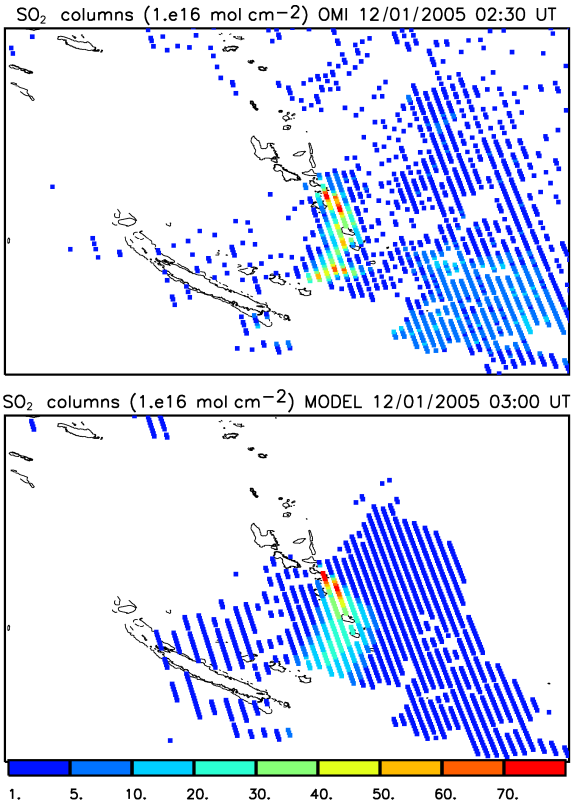

Figure 10. Top: OMI SO_2 columns (1×10^{16} molecule cm^{-2}) for the 12 January 2005 at 02:30 UTC. Bottom: simulated SO_2 columns (1×10^{16} molecule cm^{-2}) (S1_HighT) from the 10 km × 10 km grid for the 12 January 2005 at 03:00 UTC interpolated onto the OMI grid.

4.2 Impact of Ambrym on sulfate, bromine and ozone on the regional scale

Our simulations include four grids. To study impacts of Ambrym on the regional scale, model outputs for the largest grid (see Fig. 2), whose resolution is 50 km × 50 km, are analyzed. Because of computing limitations, we present only the impact for the 12 January 2005 after 11 days of spin-up.

4.2.1 Sulfate

The sulfate burden in the model domain due to Ambrym increases by 44 % (i.e., 0.08 Tg of sulfate), a value calculated as the mean difference in sulfate between S1_HighT and S0 for 12 January. The direct sulfate emission totals 3.34 Gg of sulfate since the beginning of the simulation. This means that at least 96 % (≈(80–3.34)/80 × 100) of the sulfate burden increase due to Ambrym results from the atmospheric oxidation of SO_2 from the volcano by OH. It is a lower limit as direct emissions could have left the domain during the simulation or have undergone deposition. Thus, we confirm that sulfate formed from atmospheric oxidation of SO_2 is the dominant driver of the plume halogen chemistry on the regional scale. This contrasts with the near-downwind plume where the directly emitted sulfate (formed from high-temperature SO_3) is dominant and is essential for the rapid formation of BrO (see Roberts et al., 2009; von Glasow, 2010).

Figure 11 shows the spatial distribution of sulfate due to Ambrym emissions calculated as the daily mean difference between the simulation S1_HighT and S0 for 12 January 2005. The vertical profile of this daily averaged (across the domain) sulfate is also shown in Fig. 12 for S1_HighT and S0 simulations. This figure shows that the contribution of Ambrym to the sulfate in the domain is mostly confined below 600 hPa. Figure 11 indicates that it can reach 2.5 ppbv in the plume at 875 hPa, the approximate altitude of the emissions injection in the simulation. The contribution of Am-

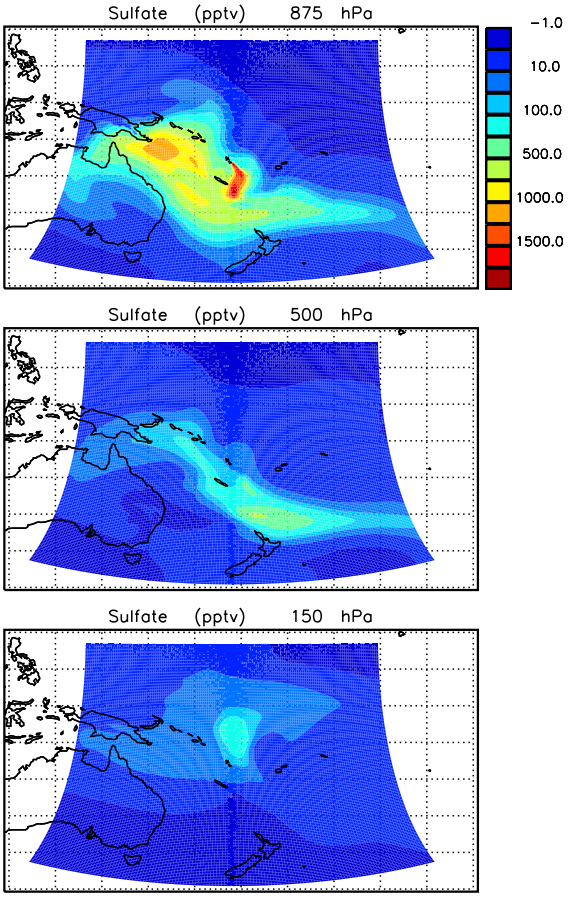

Figure 11. Daily mean difference (12 January 2005) between simulated sulfate in S1_HighT and in S0 at 875, 500 and 150 hPa for the 50 km × 50 km grid.

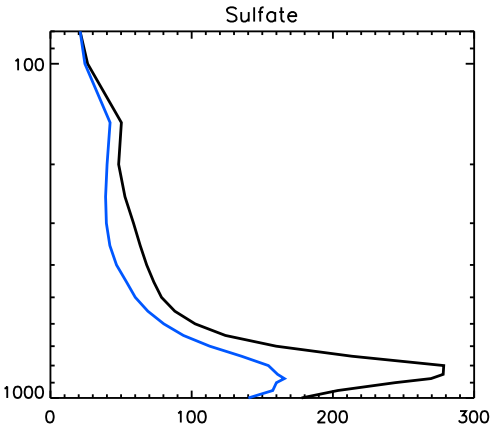

Figure 12. Profile of the daily (12 January 2005) mean mixing ratios (pptv) of sulfate simulated by the model in the larger grid (with a resolution of 50 km × 50 km) in S1_HighT (black) and in S0 (light blue).

brym is also particularly high (hundreds of pptv) in an extensive zone west of the volcano at 875 hPa. In the middle troposphere (500 hPa) and in the tropical tropopause layer (150 hPa), the influence of Ambrym is more localized. It is co-localized with convective events as can be seen in the precipitation data of the TRMM (Tropical Rainfall Measuring Mission) satellite (Huffman et al., 2007) and simulated by the model (Fig. 13). More precisely, the 500 hPa enhancement is co-localized with a band of convective systems situated southeast of New Caledonia on 12 January and in the days before. This is further confirmed by the analysis of forward trajectories initialized from Ambrym on the 10 and 11 January 2005 (Fig. 14) calculated with the HYSPLIT transport and dispersion model (Draxler and Rolph, 2003). The enhancement of sulfate at 150 hPa is co-localized with a convective event that happened north of Vanuatu on 11 January as suggested by the TRMM data (not shown) and could also result from transport from a convective event that occurred to the south as shown in Fig. 13. These localized enhancements of sulfate in the middle and upper troposphere due to Ambrym can reach 700 pptv at 500 hPa and 250 pptv at 150 hPa.

Overall, over the whole domain, above 600 hPa, the influence of Ambrym emissions is reduced: sulfate mixing ratios are increased by 30 pptv for example at 300 hPa. This is explained by the fact that sulfate aerosols are strongly washed-out by precipitation in the model. In this model study, the aqueous-phase oxidation of SO_2 to sulfate was not taken into account. This process becomes self-limiting in strong volcanic plumes due to the titration of oxidants, for example H_2O_2 (Schmidt et al., 2010), but may have a significant contribution to sulfate formation over the whole model domain, especially because the region studied is particularly cloudy, as shown by Fig. 13. Thus, this will be considered in future work.

Total aerosol optical depth (AOD) at 550 nm from MODIS Aqua is also shown in Fig. S5 of the Supplement for the 9–16 January 2005. Enhanced AOD is clearly seen southeast of Ambrym in the direction taken by the plume on the 12 January 2005 as discussed earlier (see Fig. 10) as well as northwest of Ambrym in the direction of trade winds. The latter point is again consistent with OMI SO_2 images from GSFC (Goddard Space Flight Center at http://so2.gsfc.nasa.gov/pix/daily/0105/vanuatu_0105z.html) showing that the plume was carried toward the northwest on the 14 and 15 January 2005. Figure S5 shows that enhanced AOD values vary between 0.12 and 0.34, which is approximately twice higher than the 3-year average (October 2005–October 2008) AOD from MODIS presented by Lefèvre at al. (2015). This is consistent with the extreme passive degassing activity of Ambrym during January 2005. This confirms the strong influence of Ambrym on the budget of sulfate aerosol in the southwest Pacific region and is qualitatively in agreement with our results.

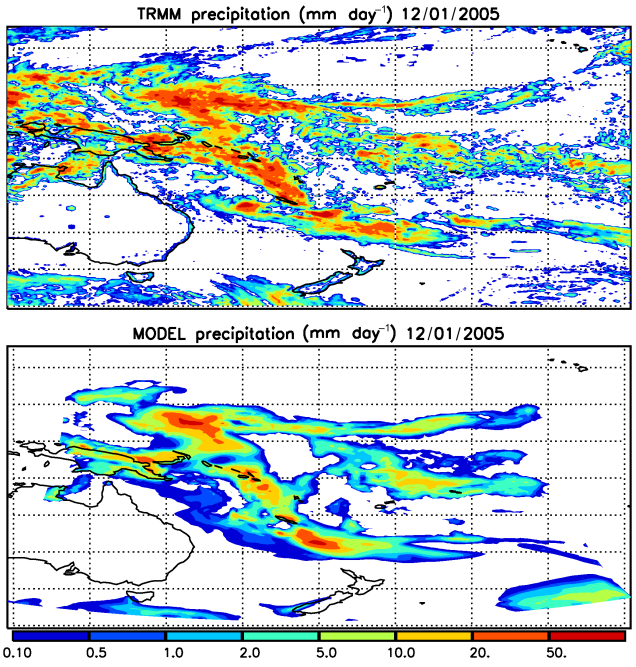

Figure 13. Daily precipitation (mm day^{-1}) for the 12 January 2005 as estimated from the TRMM satellite (3B42 product) and simulated by the model.

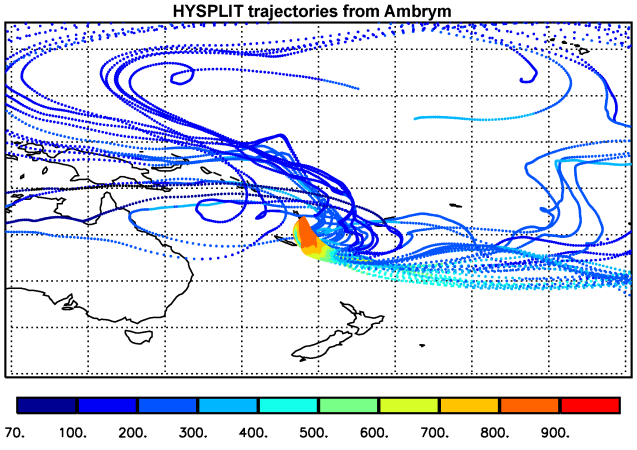

Figure 14. Fifteen-day forward trajectories initialized from the location of Ambrym Volcano at 1373 m every hour on the 10 and 11 January 2005 calculated with the HYSPLIT model. The color scale represents the pressure (in hPa) of the air masses along the trajectories.

4.2.2 Bromine

Figure 15 shows the horizontal distribution of the total bromine content ($Br_y = HBr + 2Br_2 + BrCl + Br + BrO + HOBr + BrONO_2$) due to Ambrym emissions calculated as the daily mean difference between the simulation S1_HighT and S0 for 12 January 2005. The vertical profile of this daily averaged Br_y is shown in Fig. 16 for S1_HighT and S0 simulations. The results presented here are for the larger grid, whose resolution is 50 km × 50 km. The regional influence of Ambrym Volcano emissions as a source of Br_y is clearly demonstrated. Ambrym is the main volcanic source of bromine in the domain, causing a regional plume of enhanced Br_y (maximum of 60 pptv) in the lower troposphere. Bagana Volcano in Papua New Guinea was also active at this time (see Sect. 2.3.3, "SO_2 emissions") and is responsible for a smaller enhancement in the S0 simulation around 875 hPa seen in Fig. 16. In the middle troposphere (500 hPa) and in the tropical tropopause layer (150 hPa), the influence of Ambrym is still visible but more localized, increasing the background Br_y locally by up to 3 pptv. The same convective events as those mentioned in the previous section are responsible for these Br_y enhancements. There is also evidence of transport to the stratosphere when analyzing results at 80 hPa (a model level that is above the thermal tropopause in the simulation) with a few visible patches of Br_y of up to 0.5 pptv. Such transport of volcanic bromine to the upper troposphere and the stratosphere is of strong interest. Indeed, the stratospheric bromine burden is underestimated by global models that only take into account long-lived halons and methyl bromide. The missing source is believed to arise from bromine-containing very short-lived substances (VSLSs) (i.e., bromocarbon source gases whose lifetime is less than 6 months, their degradation products and inorganic sources of bromine in the troposphere) transported from the boundary layer to the stratosphere. Their contribution to the stratospheric bromine loading ranges between 2 and 8 pptv (Carpenter et al., 2014). Here, we find that bromine emissions from Ambrym are responsible for a mean increase of 0.3 pptv of Br_y in the model domain at the altitude of the plume (875 hPa) and of 0.1 pptv around 300 hPa in the upper troposphere (Fig. 16). Local enhancements of 3 pptv are simulated in the upper troposphere due to convective transport, and there is also evidence of transport to the stratosphere (up to 80 hPa) of Br_y from Ambrym as mentioned above. Figure 16 also presents the vertical profile of daily mean Br speciation of volcanic Br_y. We have only considered the model grid boxes strongly influenced by volcanic bromine (for which the mean difference between S1_HighT and S0 was higher than 0.5 pptv in Fig. 21). It is clear from this figure that the partitioning strongly varies with altitude. In the lower troposphere, as seen previously on the local scale in Sect. 3.2, HBr is readily depleted by its conversion into reactive bromine by the reaction of HOBr on sulfate aerosol, which produces Br_2 and/or BrCl. BrCl dominates, which is surprising as it is readily photolyzed and was not found to be a major component of reactive bromine on the local plume scale (Sect. 3.2). This is most likely due to very rapid halogen cycling on sulfate aerosol, whose concentration increases as more volcanic SO_2 is oxidized in the downwind plume. HOBr also contributes to a significant fraction of Br_y on the regional scale at 875 hPa, consistent with its role as a reservoir of reactive bromine when the plume becomes diluted.

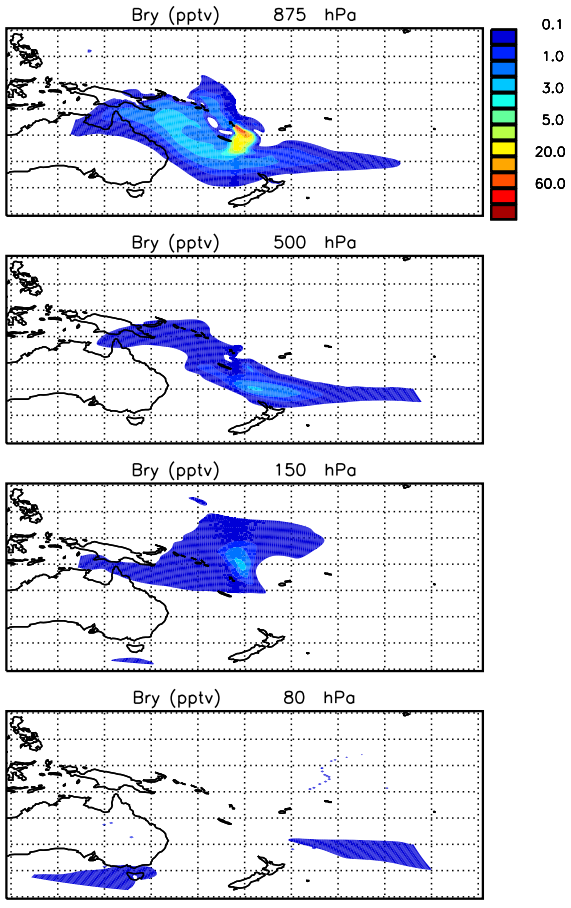

Figure 15. Daily mean difference (12 January 2005) between simulated Br_y (pptv) in S1_HighT and in S0 at 875, 500, 150 and 80 hPa for the 50 km × 50 km grid.

The greater influence of photolysis reactions at higher altitudes is shown in the profiles by the declining HOBr and increasing Br with altitude that also causes BrO to increase. HOBr can also be washed out by precipitation. There is a back-conversion of reactive bromine species (Br and BrO) into HBr at a higher altitude above 300 hPa. It is caused by reaction of volcanic Br with HO_2. Note that the difference between Br_y from S1 and from S1_HighT (not shown) is small and can reach a maximum of 3 pptv in regions of the Ambrym plume that reach up to 60 pptv Br_y at 875 hPa.

4.2.3 Ozone

Figure 17 shows the variation of ozone due to Ambrym emissions calculated as the daily mean difference in percent (of S0) between the simulation S1_HighT and S0 for 12 January 2005. The magnitude of ozone depletion in the simulation S1_HighT is correlated with the change in sulfate and in bromine due to Ambrym emissions (Figs. 11 and 15). At 875 hPa, it is at a maximum (40 %) in the concentrated plume and significant (> 10 %) in an extensive zone west of the volcano strongly influenced by Ambrym emissions (Figs. 11 and 15). Note that during the day, the depletion can be total in the plume (not shown) as presented on a plume scale (Fig. 8). Transport of an ozone-depleted air mass by convection can also be seen at 500 hPa. At higher altitudes, the influence of Ambrym on ozone mixing ratios is smaller, less than 2 %. When the whole domain is considered, Ambrym emissions are responsible for an ozone depletion of 72 Gg in the S1_HighT simulation; this represents 0.2 % of the ozone content in the domain (32 Tg of ozone). In the S1 simulation, depletion of ozone due to Ambrym totals 69 Gg of ozone. It is consistent with the fact that high-temperature chemistry initialization is only important in approximately the first 150 km from the source in our simulation as shown in Sect. 3.2.

4.3 Impact of Ambrym emissions on the oxidizing power of the troposphere

The oxidizing capacity of the troposphere determines the atmospheric fate of many atmospheric pollutants including greenhouse gases such as methane; thus, it is an important control on tropospheric composition and climate. Volcanic emissions are expected to impact the oxidizing power of the atmosphere in several ways. First, the large amounts of SO_2 emitted by volcanoes react with OH, drastically reducing its concentration. Furthermore, the conversion of emitted halogen halides to more reactive halogen species in volcanic plumes results in chemical cycles that deplete ozone and HO_2 (and therefore OH), as well as NO_x, which can in turn also affect ozone and OH. In addition, these reactive halogen cycles produce chlorine radicals that can also oxidize methane and non-methane hydrocarbons. Here, to illustrate the impact of Ambrym during the extreme degassing event of January 2005 on the oxidizing capacity of the atmosphere, we calculate the change to the lifetime of a key atmospheric greenhouse gas : methane. In particular, we investigate the relative contribution of the different components of the volcanic emissions to the overall perturbation of methane lifetime due to Ambrym degassing.

Methane is a key greenhouse gas with both natural and anthropogenic sources, whose main loss pathway from the atmosphere is by gas-phase reaction with OH. Methane lifetime due to a process (e.g., reaction with OH) is commonly defined as the total methane atmospheric burden (Tg) in steady state (i.e., with unchanged burden) divided by total methane losses through this process (Tg $year^{-1}$) (Houghton et al., 2001). We have applied this definition here. However, it is important to highlight that to calculate a proper methane lifetime, we would have to perform a simulation of about 10 years with a global model. Instead, we have calculated the instantaneous perturbation of CH_4 lifetime over the model domain (averaged over a day), which reflects the instantaneous perturbation of the methane sink on a regional scale. The results in terms of lifetime change cannot be extrapolated to the global scale and also depend strongly on the area

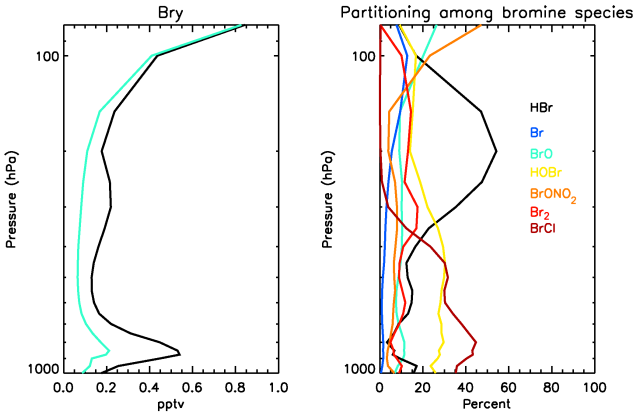

Figure 16. Left: profile of the daily (12 January 2005) mean mixing ratios of Br_y simulated by the model in the larger grid (50 km × 50 km) in S1_HighT (black) and in S0 (light blue). Right: daily mean (12 January 2005) of the Br speciation (%) for the simulation S1_HighT for grid boxes where Br_y mean difference between S1_HighT and S0 is larger than 0.5 pptv (Fig. 15).

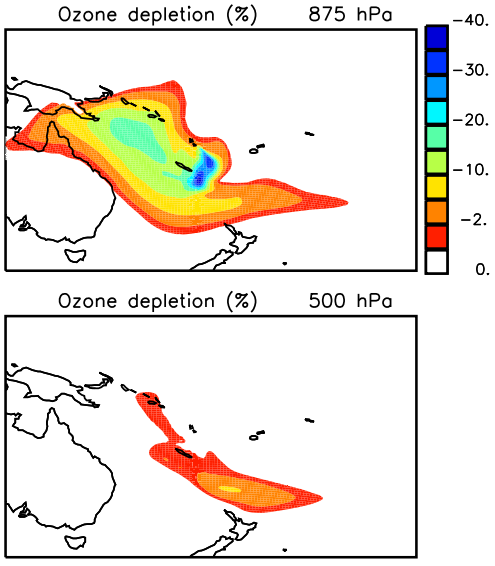

Figure 17. Daily mean difference (12 January 2005) between simulated ozone in S1_HighT and in S0 (in % relative to S0) at 875 and 500 hPa for the 50 km × 50 km grid.

of the model domain. Our aim here is to assess the relative contribution of volcanic sulfur emissions and reactive halogen plume chemistry to the overall perturbation of CH_4 lifetime.

We calculate that the methane lifetime due to the reaction of methane with OH, τ_{CH_4+OH}, is about 4.65 years in our simulation when the volcanic emission from Ambrym is not included. A value of 9.7 ± 1.5 year is derived from most recent studies based on global modeling (Naik et al., 2013). The shorter methane lifetime calculated here reflects the condition in the tropics for January where the OH concentration is particularly high. We find that τ_{CH_4+OH} increases by 0.97 % due to volcanic emissions in the simulation S1_HighT compared to the simulation S0. For the simulation with volcanic SO_2 emissions alone (S1_nohal), we calculate that the methane lifetime τ_{CH_4+OH} increase is only about 0.37 %. Therefore, the increase in methane lifetime, with respect to OH, due to volcanic emissions is enhanced by a factor of 2.6 when reactive halogen chemistry is considered.

A second consideration is that the volcano plume chlorine can itself react with methane, decreasing its lifetime. The methane lifetime due to reaction with Cl, τ_{CH_4+Cl}, is 246 years in our simulation without volcanic emission from Ambrym (S0). This compares well with the methane lifetime of about 200 years derived by Allan et al. (2007). When Ambrym emissions are included, τ_{CH_4+Cl} decreases by 17 % to 204 years due to reaction with reactive chlorine produced in Ambrym plume. Nevertheless, this reduction in methane lifetime due to Cl radicals only partially counters the increase in methane lifetime caused by the decrease in OH (through both volcanic plume halogen cycles and SO_2). The net volcanic impact is an overall 0.57 % increase in methane lifetime. Thus, the effect of chlorine radicals on the methane lifetime counteracts 41 % of the effect due to the OH decrease. Note that very recent measurements of reactive chlorine (OClO) in the Mt Etna volcanic plume (General et al., 2015; Gliß et al., 2015) could help to better quantify the impact of chlorine radicals on the methane lifetime.

4.4 Impact of Ambrym emissions on SO_2 lifetime

As already discussed in the Introduction, SO_2 undergoes atmospheric oxidation to sulfate aerosols that exert climatic impacts through both direct radiative and indirect cloud albedo effects (Schmidt et al., 2012). Sinks of SO_2 are dry and wet deposition, gas-phase oxidation and aqueous phase oxidation. The estimated lifetime of SO_2 in the troposphere by global models ranges between 0.6 and 2.6 days (e.g., Rotstayn and Lohmann, 2002, and references therein), with a lifetime with respect to gas-phase oxidation by OH of around 2 weeks (e.g., Rotstayn and Lohmann, 2002; von Glasow et al., 2009). However, model studies indicate a lengthened lifetime for volcanic SO_2 (e.g., Chin and Jacob, 1996; Graf et al., 1997; Stevenson et al., 2003; Schmidt et al., 2010). For example, a lifetime of 24–34 days was calculated for the Laki 1783–4 eruption using a global model (Schmidt et al., 2010). This is due to volcanic plume injection into the free troposphere (where removal rates are much lower than in the boundary layer) and the suppression of oxidants (OH, H_2O_2, noting the limited role of ozone under acid conditions) by the SO_2 chemistry. Our regional 3-D model study includes a less detailed SO_2–sulfate chemistry scheme (gas-phase oxidation only) but includes detailed plume reactive halogen chemistry. Here, we have calculated the impact of volcanic halo-

gen chemistry on the lifetime of SO_2 due to gas-phase oxidation by OH. More precisely, we calculate the lifetime of SO_2 in the whole domain and of SO_2 in the plume from Ambrym (defined in our study as model grids where $SO_2 > 5$ ppbv). For the simulation S1_nohal (which includes only SO_2 emissions) and for the whole domain of the simulation, we find an SO_2 lifetime of 8.8 days, consistent with previous work given that the simulation is for the tropics. For this S1_nohal simulation and considering only the plume of Ambrym, the lifetime of SO_2 increases (11 days). This is consistent with the known self-limitation of SO_2 oxidation in volcanic plumes as OH becomes depleted in the plume by the reaction with SO_2 itself. For the simulation including volcanic halogens with high-temperature initialization, S1_HighT, the SO_2 lifetime is 8 days for the whole domain and 5.5 days for the plume. This result of a shorter SO_2 lifetime in the plume than in the whole domain is initially surprising because of the self-limitation of SO_2 oxidation as explained above. The shorter SO_2 lifetimes for S1_HighT compared to S1_nohal are also again surprising because the halogen chemistry acts to further deplete OH in the plume. These results are explained by the OH emissions in S1_HighT (high-temperature initialization), which provides an additional rapid near-source sink for SO_2, thereby contributing to the effective volcanic sulfate emission. This is confirmed by the simulation, S1_nohal2 (that includes SO_2 emissions and OH emissions from HSC chemistry but no halogens), in which the SO_2 lifetimes are 7.5 days for the whole domain and 5.6 days for the plume. This impact of a high-temperature OH source on volcanic SO_2 occurs very close to the source (after which OH becomes depleted), leading to an unexpected shortening of the calculated SO_2 lifetime, which complicates the lifetime calculation. A similar effect was not seen for methane because it is not co-emitted from the volcano and OH is preferentially titrated by SO_2 (and HCl).

Because of the complication of the lifetime calculation in S1_HighT, it is better to compare the simulations with (S1) and without (S1_nohal) halogen emissions, excluding high-temperature chemistry. We have shown before that simulations with and without high-temperature chemistry give very similar results in terms of Br_y and ozone on the regional scale (see Sects. 4.2.2 and 4.2.3). In the simulation S1, the SO_2 lifetime is 15 days in the plume and 9.4 days for the whole domain. This result is consistent with what is expected as the lifetime of SO_2 is lengthened in the plume compared to the S1_nohal (SO_2 emission only) simulation (11 days). We conclude that including volcanic halogen chemistry increases the lifetime of SO_2 in the plume by 36 % through its impact on OH. Similarly, SO_2 lifetime is also increased by halogen chemistry for the whole domain but by a lesser extent (9.4 days compared to 8.8 days in S1_nohal).

5 Conclusions

The CCATT-BRAMS mesoscale model was used and further developed to study the impact of Ambrym Volcano emissions, Vanuatu (southwest Pacific), on the chemical composition of the atmosphere on the local and regional scales. We focus on an episode of extreme passive degassing of Ambrym that lasted several months in early 2005 and for which SO_2 and BrO columns from airborne DOAS measurements in the plume have been reported. Model development includes the incorporation of reactive halogen chemistry and a volcano emission source specific to Ambrym. Using the nesting grid capability of CCATT-BRAMS, we simulate the Ambrym plume at high resolution (500 m × 500 m). This allows us to make a point-by-point comparison with DOAS SO_2 and BrO data and hence test our understanding of volcanic plume chemistry at the plume level. We find that the model reproduces reasonably well the spatial distribution of SO_2 in the near-downwind plume (i.e., the direction and dilution of the plume). The model captures the salient features of volcanic chemistry as reported in previous work, such as HO_x and ozone depletion in the core of the plume. With the simulation initialized with high-temperature chemistry at the vent (which produces Br, Cl, HO_x and NO_x radical species), the pattern of a BrO / SO_2 trend with distance downwind and across the plume simulated by the model is in good agreement with the DOAS observations. However, the model underestimates by 60 % the magnitude of observed BrO columns in the near-downwind plume at 15 km. The analysis of the model results shows that BrO formation is ozone limited in the near-downwind (concentrated) plume due to the combination of a low background ozone (15 ppbv, of which 100 % is depleted in the plume) and the high emissions flux from Ambrym. Further downwind in the plume at 40 km, we find a much better agreement between observed and modeled BrO columns (mean bias of 14 %). This study confirms the importance of the high-temperature chemistry at the vent to reproduce BrO / SO_2 variation in the near-downwind plume. It also demonstrates that the (non-sulfur) radicals produced by the high-temperature chemistry are mostly important for the initial rise of BrO / SO_2 at Ambrym. Further downwind from the vents (after 150 km approximately for our case), simulations with and without the high-temperature initialization exhibit rather similar chemistry. Nevertheless, the primary aerosol emission, which is crucial to enable the heterogeneous chemistry producing reactive bromine in the near-downwind plume, originates from the high-temperature plume chemistry at the vent. It was kept constant in these simulations (at 1 % of total sulfur), and hence its impact is not taken into account when comparing simulations with and without high-temperature chemistry.

Our 3-D regional model approach allows us to make the link between near-downwind plume observations and regional-scale observations given by satellite data. Here, we show that the model when initialized with the Ambrym SO_2

source strength estimate derived from the DOAS observations by Bani et al. (2009, 2012) simulates SO_2 columns on the regional scale that agree within 25 % with the SO_2 columns detected by OMI. Impacts of Ambrym in the southwest Pacific region were also analyzed across the larger model grid domain. In the lower troposphere, at altitudes close to the injection height (875 hPa), Ambrym causes a substantial increase in sulfate (from 0.1 to 2.5 ppbv) and in bromine mixing ratios (from 0.1 to 60 pptv). The transport of bromine species (as well as sulfate) to the upper troposphere due to convection is also predicted by the model, with convective regions confirmed by the precipitation data from the TRMM satellite as well as by trajectories from the HYSPLIT transport and dispersion model. There is also evidence in the simulations of a subsequent transport of bromine to the stratosphere from Ambrym. Thus, the halogen activation in tropospheric volcanic plumes could be one aspect of the potential impact of volcanic halogen on stratospheric ozone. In future work, longer-duration simulations should be performed to fully quantify the impact of Ambrym on the chemical composition of the troposphere on the regional scale. In particular, the flux of bromine to the upper troposphere and to the stratosphere from this extreme continuous degassing event, as well as during the typical continuous emission from Ambrym, should be calculated. This will provide an insight into the importance of the Ambrym Volcano plume for the budget and chemistry of bromine in these regions. Ozone depletion (between 5 and 40 %) is ongoing, albeit slower in the extensive region a few thousands of kilometers from the volcano influenced by the dispersed plume. We find a tropospheric ozone depletion of 72 Gg, (i.e., 0.2 % for a domain containing 32 Tg of ozone) in the model domain.

This influence of the plume chemistry on tropospheric oxidants (depletion of HO_x and ozone by reactive halogen chemistry and depletion of OH by oxidation of SO_2) in turn affects other atmospheric species in the model. We show that methane lifetime (with respect to its reaction with OH and with Cl) in the model is increased when volcanic emissions are taken into account, confirming the potential for volcanic emissions to influence the oxidizing power of the atmosphere. Furthermore, the increase in methane lifetime, with respect to oxidation by OH, due to volcanic emissions is enhanced by a factor of 2.6 when reactive halogen chemistry is considered. Cl radicals produced in the plume counteract some of the effect (41 %) of the methane lifetime lengthening due to OH depletion. This work thereby particularly highlights the impact of reactive volcanic halogen chemistry on the oxidizing capacity of the atmosphere. Here, it is found to be more important than the impact of OH depletion by volcanic SO_2. However, the reactive halogen-mediated HO_x depletion and Cl radical formation have opposing impacts on the methane lifetime. Furthermore, we calculate an increase of 36 % in the SO_2 lifetime with respect to oxidation by OH when reactive halogen chemistry in the plume is included in the simulations. Thus, reactive halogen chemistry exerts a significant influence on the volcanic SO_2 lifetime and hence also on the production of sulfate. This needs to be taken into account in studies evaluating the impact of volcanoes on radiative forcing, especially if the injection height is high in altitude (where the sink of SO_2 by OH can be the dominant oxidation pathway and thus exert a major control on SO_2 lifetime and sulfate formation; Schmidt et al., 2010). Washout processes were included in the model, but the aqueous phase of oxidation of SO_2 was not. In future this should also be included in the model, given the cloudiness of the Vanuatu region.

Uncertainties in the modeled plume chemistry include aspects of the volcanic emissions and also the rate of heterogeneous reaction of HOBr on the volcanic aerosol, which is a key driver of the reactive halogen cycling and hence of the plume regional impacts. This depends on the aerosol surface area and underlying chemical kinetics (for which a reevaluation for acidic plume conditions was made by Roberts et al., 2014b). Ongoing work is aimed at improving the aerosol and HOBr reactive uptake parameterization in the model.

Transects across the plume at various distances from the vents, as performed by Bani et al. (2009), appear very useful altogether with a model to test our understanding of the dynamics of volcanic plume chemistry. Nevertheless, this study emphasizes the need to measure more chemical species to constrain knowledge of the volcanic plume chemistry as also highlighted in Bobrowski et al. (2015). In particular, the coupling between BrO_x ($= Br + BrO$) and NO_x appears rather uncertain (Roberts et al., 2014a). Measurements of BrO and SO_2 are not sufficient to fully constrain the plume chemistry; background ozone as well as in-plume ozone, HO_x, NO_x and bromine compounds other than BrO and size-resolved aerosol characterization are needed along with a better characterization of the plume injection height and of the plume depth (width in general being constrained by satellite and DOAS transects). To be most insightful, studies should combine the systematic downwind plume investigation with (simultaneous) detailed crater-rim measurements to constrain the volcanic gas and aerosol emission. Recent advances in the satellite detection of reactive halogen species in tropospheric volcanic plumes (Hörmann et al., 2013) may also be used in future regional and global model studies of volcanic activity impacts.

6 Data availability

Model simulations presented in this manuscript are available on request from the corresponding author.

The Supplement related to this article is available online at doi:10.5194/acp-16-12099-2016-supplement.

Acknowledgements. This work was supported by the LABEX VOLTAIRE (VOLatils – Terre Atmosphère Interactions – Ressources et Environnement) ANR-10-LABX-100-01 (2011–20). It also benefited from the financial support of the program LEFE of the Institut National des Sciences de l'Univers of CNRS (Centre National de la Recherche Scientifique) provided to the HEVA project. The authors benefitted from the use of the cluster at the Centre de Calcul Scientifique en région Centre. We gratefully acknowledge Saulo Freitas (NOAA/ESRL/CPTEC) for his help with the CCATT-BRAMS model and Laurent Catherine (OSUC) for technical help with the cluster at Centre de Calcul Scientifique en région Centre. We thank P. Bani (IRD) and C. Oppenheimer (University of Cambridge) for providing their DOAS data, Virginie Marécal (CNRM/Météo-France) for initiating the project, and Bruno Scaillet (ISTO) for providing some earlier HCl / SO_2 and HBr / SO_2 ratios. We are grateful to the NOAA Air Resources Laboratory for the provision of the HYSPLIT Transport and dispersion model (http://ready.arl.noaa.gov/HYSPLIT_hytrial.php).

Edited by: M. Van Roozendael
Reviewed by: two anonymous referees

References

Aiuppa, A., Federico, C., Franco, A., Giudice, G., Gurrieri, S., Inguaggiato, S., Liuzzo, M., McGonigle, A. J. S., and Valenza, M.: Emission of bromine and iodine from Mount Etna volcano, Geochem. Geophy. Geosys., 6, Q08008, doi:10.1029/2005GC000965, 2005.

Allan, W., Struthers, H., and Lowe, D. C.: Methane carbon isotope effects caused by atomic chlorine in the marine boundary layer: Global model results compared with Southern Hemisphere measurements, J. Geophys. Res., 112, D04306, doi:10.1029/2006JD007369, 2007.

Allard, P., Aiuppa, A., Bani, P., Metrich, N., Bertagnini, A., Gauthier, P. J., Parelli, F., Sawyer, G. M., Shinohara, H., Bagnator, E., Mariet, C., Garebiti, E., and Pelletier, B.: Ambrym basaltic volcano (Vanuatu Arc): volatile fluxes, magma degassing rate and chamber depth, in: AGU Fall Meeting Abstracts, Vol. 1, San Francisco, United States of America, December 2009.

Allard, P., Aiuppa, A., Bani, P., Métrich, N., Bertagnini, A., Gauthier, P. J., Shinohara, H., Sawyer, G., Parello, F., Bagnato, E., and Pelletier, B.: Prodigious emission rates and magma degassing budget of major, trace and radioactive volatile species from Ambrym basaltic volcano, Vanuatu island Arc, J. Volcanol. Geoth. Res., doi:10.1016/j.jvolgeores.2015.10.004, online first, 2015.

Allibone, R., Cronin, S. J., Douglas, C. T., Oppenheimer, C., Neall, V. E., and Stewart, R. B.: Dental fluorosis linked to degassing on Ambrym volcano, Vanuatu: a novel exposure, pathway, Environ. Geochem. Hlth., 34, 155–170, doi:10.1007/s10653-010-9338-2, 2010.

Andres, R. J. and Kasgnoc A. D.: A time-averaged inventory of subaerial volcanic sulfur emissions, J. Geophys. Res.-Atmos., 103, 25251–25261, 1998.

Arteta, J., Marécal, V., and Rivière, E. D.: Regional modelling of tracer transport by tropical convection – Part 1: Sensitivity to convection parameterization, Atmos. Chem. Phys., 9, 7081–7100, doi:10.5194/acp-9-7081-2009, 2009a.

Arteta, J., Marécal, V., and Rivière, E. D.: Regional modelling of tracer transport by tropical convection – Part 2: Sensitivity to model resolutions, Atmos. Chem. Phys., 9, 7101–7114, doi:10.5194/acp-9-7101-2009, 2009b.

Atkinson, R., Baulch, D. L., Cox, R. A., Crowley, J. N., Hampson, R. F., Hynes, R. G., Jenkin, M. E., Rossi, M. J., and Troe, J.: Evaluated kinetic and photochemical data for atmospheric chemistry: Volume III – gas phase reactions of inorganic halogens, Atmos. Chem. Phys., 7, 981–1191, doi:10.5194/acp-7-981-2007, 2007.

Bani, P.: Caractérisation et suivi du dégazage des principaux édifices volcaniques actifs de l'arc insulaire du Vanuatu par télédetection, PhD thesis of Université de la Nouvelle-Calédonie, 2006.

Bani, P., Oppenheimer, C., Tsanev, V. I., Carn, S. A., Cronin, S. J., Crimp, R., Calkins, J. A., Charley, D., Lardy, M. and Roberts, T. R.: Surge in sulph ur and halogen degassing from Ambrym volcano, Vanuatu, B. Volcanol., 71, 1159–1168, 2009.

Bani, P., Oppenheimer, C., Allard, P., Shinohara, H., Tsanev, V., Carn, S., Lardy, M., and Garaebiti, E.: First estimate of volcanic SO_2 budget for Vanuatu island arc, J. Volcanol. Geoth. Res., 211, 36–46, 2012.

Barrie, L. A., Bottenheim, J. W., Schnell, R. C., Crutzen, P. J., and Rasmussen, R. A.: Ozone Destruction and Photochemical Reactions at Polar Sunrise in the Lower Arctic Atmosphere, Nature, 334, 138–141, doi:10.1038/334138a0, 1988.

Bela, M. M., Longo, K. M., Freitas, S. R., Moreira, D. S., Beck, V., Wofsy, S. C., Gerbig, C., Wiedemann, K., Andreae, M. O., and Artaxo, P.: Ozone production and transport over the Amazon Basin during the dry-to-wet and wet-to-dry transition seasons, Atmos. Chem. Phys., 15, 757–782, doi:10.5194/acp-15-757-2015, 2015.

Bhartia, P. K. and Wellemeyer, C. W.: OMI TOMS-V8 Total O3 Algorithm, Algorithm Theoretical Baseline Document: OMI Ozone Products, edited by: Bhartia, P. K., Vol. II, ATBD-OMI-02,version 2.0, available at: http://eospso.gsfc.nasa.gov/sites/default/files/atbd/ATBD-OMI-02.pdf (last access: November 2015), 2002.

Bobrowski, N. and Platt, U.: SO_2 / BrO ratios studied in five volcanic plumes, J. Volcanol. Geoth. Res., 166, 147–160, 2007.

Bobrowski, N., Hönninger, G., Galle, B., and Platt, U.: Detection of bromine monoxide in a volcanic plume, Nature, 423, 273–276, 2003.

Bobrowski, N., von Glasow, R., Aiuppa, A., Inguaggiato, S., Louban, I., Ibrahim, O. W., and Platt, U.: Reactive halogen chemistry in volcanic plumes, J. Geophys. Res., 112, D06311, doi:10.1029/2006JD007206, 2007.

Bobrowski, N., Glasow, R., Giuffrida, G. B., Tedesco, D., Aiuppa, A., Yalire, M., Arellano, S., Johansson, M., and Galle, B.: Gas emission strength and evolution of the molar ratio of BrO / SO_2 in the plume of Nyiragongo in comparison to Etna, J. Geophys. Res.-Atmos., 120, 277–291, 2015.

Boichu, M., Oppenheimer, C., Roberts, T. J., Tsanev, V., and Kyle, P. R.: On bromine, nitrogen oxides and ozone depletion in the tropospheric plume of Erebus volcano (Antarctica), Atmos. Environ., 45, 3856–3866, 2011.

Cadoux, A., Scaillet, B., Bekki, S., Oppenheimer, C., and Druitt, T. H.: Stratospheric Ozone destruction by the Bronze-Age Mi-

noan eruption (Santorini Volcano, Greece), Sci. Rep., 5, 12243, doi:10.1038/srep12243, 2015.

Carn, S. A., Clarisse, L., and Prata, A. J.: Multi-decadal satellite measurements of global volcanic degassing, J. Volcanol. Geoth. Res., 311, 99–134, doi:10.1016/j.jvolgeores.2016.01.002, 2016.

Carpenter L. J., Reimann, S., Burkholder, J. B., Clerbaux, C., Hall, B. D., Hossaini, R., Laube, J. C., and Yvon-Lewis, S. A.: Ozone-Depleting Substances (ODSs) and Other Gases of Interest to the Montreal Protocol, chap. 1 in: Scientific Assessment of Ozone Depletion: 2014, Global Ozone Research and Monitoring Project – Report No. 55, World Meteorological Organization, Geneva, Switzerland, 2014.

Carslaw, K. S., Lee, L. A., Reddington, C. L., Pringle, K. J., Rap, A., Forster, P. M., Mann, G. W., Spracklen, D. V., Woodhouse, M. T., Regayre, L. A., and Pierce, J. R.: Large contribution of natural aerosols to uncertainty in indirect forcing, Nature, 503, 67–71, 2013.

Chin, M. and Jacob, D. J.: Anthropogenic and natural contributions to tropospheric sulfate: A global model analysis, J. Geophys. Res.-Atmos., 101, 18691–18699, 1996.

Delmelle, P.: Environmental impacts of tropospheric volcanic gas plumes, Special Publication – Geological Society of London, 213, 381–400, 2003.

Diehl, T., Heil, A., Chin, M., Pan, X., Streets, D., Schultz, M., and Kinne, S.: Anthropogenic, biomass burning, and volcanic emissions of black carbon, organic carbon, and SO_2 from 1980 to 2010 for hindcast model experiments, Atmos. Chem. Phys. Discuss., 12, 24895–24954, doi:10.5194/acpd-12-24895-2012, 2012.

Draxler, R. R. and Rolph, G. D.: HYSPLIT (HYbrid Single-Particle Lagrangian Integrated Trajectory) Model access via NOAA ARL READY Website, available at: http://ready.arl.noaa.gov/HYSPLIT.php (last access: November 2015), 2003.

Fan, S.-M. and Jacob, D. J.: Surface ozone depletion in Arctic spring sustained by bromine reactions on aerosols, Nature, 359, 522–524, 1992.

Freitas, S. R., Longo, K. M., Silva Dias, M. A. F., Chatfield, R., Silva Dias, P., Artaxo, P., Andreae, M. O., Grell, G., Rodrigues, L. F., Fazenda, A., and Panetta, J.: The Coupled Aerosol and Tracer Transport model to the Brazilian developments on the Regional Atmospheric Modeling System (CATT-BRAMS) – Part 1: Model description and evaluation, Atmos. Chem. Phys., 9, 2843–2861, doi:10.5194/acp-9-2843-2009, 2009.

Freitas, S. R., Longo, K. M., Alonso, M. F., Pirre, M., Marecal, V., Grell, G., Stockler, R., Mello, R. F., and Sánchez Gácita, M.: PREP-CHEM-SRC – 1.0: a preprocessor of trace gas and aerosol emission fields for regional and global atmospheric chemistry models, Geosci. Model Dev., 4, 419–433, doi:10.5194/gmd-4-419-2011, 2011.

General, S., Bobrowski, N., Pöhler D., Weber, K., Fischer, C., and Platt, U.: Airborne I-DOAS measurements at Mt. Etna: BrO and OClO evolution in the plume, J. Volcanol. Geoth. Res., 300, 175–186, doi:10.1016/j.jvolgeores.2014.05.012, 2015.

Gerlach, T. M.: Volcanic sources of tropospheric ozone-depleting trace gases, Geochem. Geophy. Geosys., 5, Q09007, doi:10.1029/2004GC000747, 2004.

Gliß, J., Bobrowski, N., Vogel, L., Pöhler, D., and Platt, U.: OClO and BrO observations in the volcanic plume of Mt. Etna – implications on the chemistry of chlorine and bromine species in volcanic plumes, Atmos. Chem. Phys., 15, 5659–5681, doi:10.5194/acp-15-5659-2015, 2015.

Graf, H. F., Feichter, J., and Langmann, B.: Volcanic sulfur emissions: Estimates of source strength and its contribution to the global sulfate distribution, J. Geophys. Res.-Atmos., 102, 10727–10738, 1997.

Grellier, L., Marécal, V., Josse, B., Hamer, P. D., Roberts, T. J., Aiuppa, A., and Pirre, M.: Towards a representation of halogen chemistry within volcanic plumes in a chemistry transport model, Geosci. Model Dev. Discuss., 7, 2581–2650, doi:10.5194/gmdd-7-2581-2014, 2014.

Guenther, A., Karl, T., Harley, P., Wiedinmyer, C., Palmer, P. I., and Geron, C.: Estimates of global terrestrial isoprene emissions using MEGAN (Model of Emissions of Gases and Aerosols from Nature), Atmos. Chem. Phys., 6, 3181–3210, doi:10.5194/acp-6-3181-2006, 2006.

Halmer, M. M., Schmincke, H.-U., and Graf, H.-F.: The annual volcanic gas input into the atmosphere, in particular into the stratosphere: a global data set for the past 100 years, J. Volcanol. Geoth. Res., 115, 511–528, 2002.

Hebestreit, K., Stutz, J., Rosen, D., Matveiv, V., Peleg, M., Luria, M., and Platt, U.: DOAS measurements of tropospheric bromine oxide in mid-latitudes, Science, 283, 55–57, 1999.

Hörmann, C., Sihler, H., Bobrowski, N., Beirle, S., Penning de Vries, M., Platt, U., and Wagner, T.: Systematic investigation of bromine monoxide in volcanic plumes from space by using the GOME-2 instrument, Atmos. Chem. Phys., 13, 4749–4781, doi:10.5194/acp-13-4749-2013, 2013.

Houghton, J., Ding, Y., Griggs, D. J., Noguer, M., van der Linden P. J., Dai, X., Maskell, K., and Johnson, C. A. (Eds.): IPCC 2001: Climate Change 2001, Cambridge University Press, Cambridge, England, 2001.

Huffman, G. J., Adler, R. F., Bolvin, D. T., Gu, G., Nelkin, E. J., Bowman, K. P., Hong, Y., Stocker, E. F., and Wolff, D. B.: The TRMM Multi-satellite Precipitation Analysis: Quasi-Global, Multi-Year, Combined-Sensor Precipitation Estimates at Fine Scale, J. Hydrometeor., 8, 38–55, 2007.

Hunton, D. E., Viggiano, A. A., Miller, T. M., Ballenthin, J. O., Reeves, J. M., Wilson, J. C., Lee, S.-H., Anderson, B. E., Brune, W. H., Harder, H., Simpas, J. B., and Oskarsson, N.: Insitu aircraft observations of the 2000 Mt. Hekla volcanic cloud: Composition and chemical evolution in the Arctic lower stratosphere, J. Volcanol. Geoth. Res., 145, 23–34, 2005.

Josse, B., Simon, P., and Peuch, V.-H.: Radon global simulations with the multiscale chemistry and transport model MOCAGE, Tellus B, 56, 339–356, 2004.

Kelly, P. J., Kern, C., Roberts, T. J., Lopez, T., Werner, C., and Aiuppa, A.: Rapid chemical evolution of tropospheric volcanic emissions from Redoubt Volcano, Alaska, based on observations of ozone and halogen-containing gases, J. Volcanol. Geoth. Res., 259, 317–333, 2013.

Kern, C., Sihler, H., Vogel, L., Rivera, C., Herrera, M., and Platt, U.: Halogen oxide measurements at Masaya Volcano, Nicaragua using active long path differential optical absorption spectroscopy, B. Volcanol., 71, 659–670, 2009.

Lee, C., Kim, Y. J., Tanimoto, H., Bobrowski, N., Platt, U., Mori, T., Yamamoto, K., and Hong, C. S.: High ClO and ozone depletion observed in the plume of Sakurajima volcano, Japan, Geophys. Res. Lett., 32, L21809, doi:10.1029/2005GL023785, 2005.

Lefèvre, J., Menkes, C., Bani, P., Marchesiello, P., Curci, G., Grell, G., and Frouin, R.: Distribution of sulfur aerosol precursors in the SPCZ released by continuous volcanic degassing at Ambrym, Vanuatu, J. Volcanol. Geoth. Res., doi:10.1016/j.jvolgeores.2015.07.018, online first, 2015.

Li, C., Joiner, J., Krotkov, N. A., and Bhartia, P. K.: A fast and sensitive new satellite SO_2 retrieval algorithm based on principal component analysis: Application to the ozone monitoring instrument, Geophys. Res. Lett., 40, 6314–6318, doi:10.1002/2013GL058134, 2013.

Logan, J. A.: An analysis of ozonesonde data for the troposphere: Recommendations for testing 3-D models and development of a gridded climatology for tropospheric ozone, J. Geophys. Res., 104, 16115–16149, doi:10.1029/1998JD100096, 1999.

Longo, K. M., Freitas, S. R., Pirre, M., Marécal, V., Rodrigues, L. F., Panetta, J., Alonso, M. F., Rosário, N. E., Moreira, D. S., Gácita, M. S., Arteta, J., Fonseca, R., Stockler, R., Katsurayama, D. M., Fazenda, A., and Bela, M.: The Chemistry CATT-BRAMS model (CCATT-BRAMS 4.5): a regional atmospheric model system for integrated air quality and weather forecasting and research, Geosci. Model Dev., 6, 1389–1405, doi:10.5194/gmd-6-1389-2013, 2013.

Marécal, V., Pirre, M., Krysztofiak, G., Hamer, P. D., and Josse, B.: What do we learn about bromoform transport and chemistry in deep convection from fine scale modelling?, Atmos. Chem. Phys., 12, 6073–6093, doi:10.5194/acp-12-6073-2012, 2012.

Martin, R. S., Mather, T. A., and Pyle, D. M.: High-temperature mixtures of magmatic and atmospheric gases, Geochem. Geophy. Geosys., 7, Q04006, doi:10.1029/2005GC001186, 2006.

Martin, R. S., Roberts, T. J., Mather, T. A., and Pyle, D. M.: The implications of H_2S and H_2 kinetic stability in high-T mixtures of magmatic and atmospheric gases for the production of oxidized trace species (eg, BrO and NO_x), Chem. Geol., 263, 143–159, 2009.

Martin, R. S., Ilyinskaya, E., and Oppenheimer C.: The enigma of reactive nitrogen in volcanic emissions, Geochim. Cosmochim. Ac., 95, 93–105, 2012.

Mather, T. A., Allen, A. G., Oppenheimer, C., Pyle, D. M., and McGonigle, A. J. S.: Size-resolved characterisation of soluble ions in the particles in the tropospheric plume of Masaya volcano, Nicaragua: Origins and plume processing, J. Atmos. Chem., 46, 207–237, 2003.

Mather, T. A, Pyle, D. M., and Allen, A. G.: Volcanic source for fixed nitrogen in the early Earth's atmosphere, Geology, 32, 905–908, doi:10.1130/G20679.1, 2004.

Millard, G. A., Mather, T. A., Pyle, D. M., Rose, W. I., and Thornton, B.: Halogen emissions from a small volcanic eruption: Modeling the peak concentrations, dispersion, and volcanically induced ozone loss in the stratosphere. Geophys. Res. Lett., 33, L19815, doi:10.1029/2006GL026959, 2006.

Mosca, S. G., Graziani, W., and Klug, R., and Bellasio, B. R.: A statistical methodology for the evaluation of long-range dispersion models: An application to the ETEX exercise, Atmos. Environ., 32, 4302–4324, 1998.

Myhre, G., Shindell, D., Bréon, F.-M., Collins, W., Fuglestvedt, J., Huang, J., Koch, D., Lamarque, J.-F., Lee, D., Mendoza, B., Nakajima, T., Robock, A., Stephens, G., Takemura, T., and Zhang, H.: Anthropogenic and Natural Radiative Forcing, in: Climate Change 2013: The Physical Science Basis. Contribution of Working Group I to the Fifth Assessment Report of the Intergovernmental Panel on Climate Change, edited by: Stocker, T. F., Qin, D., Plattner, G.-K., Tignor, M., Allen, S. K., Boschung, J., Nauels, A., Xia, Y., Bex, V., and Midgley, P. M., Cambridge University Press, Cambridge, United Kingdom and New York, NY, USA, 2013.

Naik, V., Voulgarakis, A., Fiore, A. M., Horowitz, L. W., Lamarque, J.-F., Lin, M., Prather, M. J., Young, P. J., Bergmann, D., Cameron-Smith, P. J., Cionni, I., Collins, W. J., Dalsøren, S. B., Doherty, R., Eyring, V., Faluvegi, G., Folberth, G. A., Josse, B., Lee, Y. H., MacKenzie, I. A., Nagashima, T., van Noije, T. P. C., Plummer, D. A., Righi, M., Rumbold, S. T., Skeie, R., Shindell, D. T., Stevenson, D. S., Strode, S., Sudo, K., Szopa, S., and Zeng, G.: Preindustrial to present-day changes in tropospheric hydroxyl radical and methane lifetime from the Atmospheric Chemistry and Climate Model Intercomparison Project (ACCMIP), Atmos. Chem. Phys., 13, 5277–5298, doi:10.5194/acp-13-5277-2013, 2013.

Oppenheimer, C., Tsanev, V. I., Braban, C. F., Cox, R. A., Adams, J. W., Aiuppa, A., Bobrowski, N., Delmelle, P., Barclay, J., and McGonigle, A. J. S.: BrO formation in volcanic plumes, Geochim. Cosmochim. Ac., 70, 2935–2941, 2006.

Oppenheimer, C., Kyle, P., Eisele, F., Crawford, J., Huey, G., Tanner, D., Kim, S., Maudlin, L., Blake, D., Beyersdorf, A., Bubr, M., and Davis, D.: Atmospheric chemistry of an Antarctic volcanic plume, J. Geophys. Res., 115, D04303, doi:10.1029/2009JD011910, 2010.

Putirka, K. D.: Thermometers and barometers for volcanic systems, in: Minerals, Inclusions and Volcanic Processes, edited by: Putirka, K. D. and Tepley, F., Reviews in Mineralogy and Geochemistry 69, 61–120, 2008.

Prata, A. J., Carn, S. A., Stohl, A., and Kerkmann, J.: Long range transport and fate of a stratospheric volcanic cloud from Soufrière Hills volcano, Montserrat, Atmos. Chem. Phys., 7, 5093–5103, doi:10.5194/acp-7-5093-2007, 2007.

Pyle, D. M. and Mather, T. A.: Halogens in igneous processes and their fluxes to the atmosphere and oceans from volcanic activity: a review, Chem. Geol., 263, 110–121, 2009.

Remer, L. A., Kaufman, Y. J., Tanre, D., Mattoo, S., Chu, D. A., Martins, J. V., Li, R. R., Ichoku, C., Levy, R. C., Kleidman, R. G., Eck, T. F., Vermote, E., and Holben, B. N.: The MODIS aerosol algorithm, products, and validation, J. Atmos. Sci., 62, 947–973, 2005.

Remer, L. A., Kleidman, R. G., Levey, R. C., Kaufmann, Y. J., Tanré, D., Mattoo, S., Martins, J. V., Ichoku, C., Koren, I., Yu, H., and Holben, B. N.: Global aerosol climatology from the MODIS satellite sensors, J. Geophys. Res., 113, D14S07, doi:10.1029/2007JD009661, 2008.

Roberts, T. J., Braban, C. F., Martin, R. S., Oppenheimer, C., Adams, J. W., Cox, R. A., Jones, R. L., and Griffiths, P. T.: Modelling reactive halogen formation and ozone depletion in volcanic plumes, Chem. Geol., 263, 151–163, 2009.

Roberts, T. J., Martin, R. S., and Jourdain, L.: Reactive bromine chemistry in Mount Etna's volcanic plume: the influence of total Br, high-temperature processing, aerosol loading and plume-air mixing, Atmos. Chem. Phys., 14, 11201–11219, doi:10.5194/acp-14-11201-2014, 2014a.

Roberts, T. J., Jourdain, L., Griffiths, P. T., and Pirre, M.: Re-evaluating the reactive uptake of HOBr in the troposphere with

implications for the marine boundary layer and volcanic plumes, Atmos. Chem. Phys., 14, 11185–11199, doi:10.5194/acp-14-11185-2014, 2014b.

Robin, C., Eissen, J.-P., and Monzier, M.: Giant tuff cone and 12-kin-wide associated caldera at Ambrym Volcano (Vanuatu, New Hebrides Arc), J. Volcanol. Geoth. Res., 55, 225–238, 1993.

Roine, A.: HSC Chemistry 6.1, Tech. rep., Outotec Research Oy, Pori, Finland, 2007.

Rosário, N. E., Longo, K. M., Freitas, S. R., Yamasoe, M. A., and Fonseca, R. M.: Modeling the South American regional smoke plume: aerosol optical depth variability and surface shortwave flux perturbation, Atmos. Chem. Phys., 13, 2923–2938, doi:10.5194/acp-13-2923-2013, 2013.

Rose, W. I., Millard G. A., Mather T. A., Hunton D. E., Anderson B., Oppenheimer C., Thornton B. F., Gerlach T. M., Viggiano A. A., Kondo Y., Miller T. M., and Ballenthin J. O.: Atmospheric chemistry of a 33–34 hour old volcanic cloud from Hekla Volcano (Iceland): Insights from direct sampling and the application of chemical box modeling, J. Geophys. Res., 111, D20206, doi:10.1029/2005JD006872, 2006.

Rotstayn, L. D. and Lohmann, U.: Simulation of the tropospheric sulfur cycle in a global model with a physically based cloud scheme, J. Geophys. Res., 107, 4592, doi:10.1029/2002JD002128, 2002.

Saiz-Lopez, A., Plane, J. M. C., and Shillito, J. A.: Bromine oxide in the mid-latitude marine boundary layer, Geophys. Res. Lett., 31, L03111, doi:10.1029/2003GL018956, 2004.

Sander, R.: Compilation of Henry's Law Constants for Inorganic and Organic Species of Potential Importance in Environmental Chemistry, available at: http://www.henrys-law.org/henry-3.0.pdf (last access: November 2015), 1999.

Sander, S. P., Friedl, R. R., Golden, D. M., Kurylo, M. J., Moortgat, G. K., Keller-Rudek, H., Wine, P. H., Ravishankara, A. R., Kolb, C. E., Molina, M. J., Finlayson-Pitts, B. J., Huie, R. E., and Orkin, V. L.: Chemical Kinetics and Photochemical Data for Use in Atmospheric Studies, Evaluation Number 15, JPL Publication 06-2, Jet Propulsion Laboratory, Pasadena, CA, available at: http://jpldataeval.jpl.nasa.gov/pdf/JPL_15_AllInOne.pdf (last access: November 2015), 2006.

Schmidt, A., Carslaw, K. S., Mann, G. W., Wilson, M., Breider, T. J., Pickering, S. J., and Thordarson, T.: The impact of the 1783–1784 AD Laki eruption on global aerosol formation processes and cloud condensation nuclei, Atmos. Chem. Phys., 10, 6025–6041, doi:10.5194/acp-10-6025-2010, 2010.

Schmidt, A., Carslaw, K. S., Mann, G. W., Rap, A., Pringle, K. J., Spracklen, D. V., Wilson, M., and Forster, P. M.: Importance of tropospheric volcanic aerosol for indirect radiative forcing of climate, Atmos. Chem. Phys., 12, 7321–7339, doi:10.5194/acp-12-7321-2012, 2012.

Schultz, M., Backman, L., Balkanski, Y., Bjoerndalsaeter, S., Brand, R., Burrows, J., Dalsoeren, S., de Vasconcelos, M., Grodtmann, B., Hauglustaine, D., Heil, A., Hoelzemann, J., Isaksen, I., Kaurola, J., Knorr, W., Ladstaetter-Weienmayer, A., Mota, B., Oom, D., Pacyna, J., Panasiuk, D., Pereira, J., Pulles, T., Pyle, J., Rast, S., Richter, A., Savage, N., Schnadt, C., Schulz, M., Spessa, A., Staehelin, J., Sundet, J., Szopa, S., Thonicke, K., van het Bolscher, M., van Noije, T., van Velthoven, P., Vik, A., and Wittrock, F.: REanalysis of the TROpospheric chemical composition over the past 40 years (RETRO). A long-term global modeling study of tropospheric chemistry, Final Report, Tech. rep., Max Planck Institute for Meteorology, Hamburg, Germany, 2007.

Schumann, U., Weinzierl, B., Reitebuch, O., Schlager, H., Minikin, A., Forster, C., Baumann, R., Sailer, T., Graf, K., Mannstein, H., Voigt, C., Rahm, S., Simmet, R., Scheibe, M., Lichtenstern, M., Stock, P., Rüba, H., Schäuble, D., Tafferner, A., Rautenhaus, M., Gerz, T., Ziereis, H., Krautstrunk, M., Mallaun, C., Gayet, J.-F., Lieke, K., Kandler, K., Ebert, M., Weinbruch, S., Stohl, A., Gasteiger, J., Groß, S., Freudenthaler, V., Wiegner, M., Ansmann, A., Tesche, M., Olafsson, H., and Sturm, K.: Airborne observations of the Eyjafjalla volcano ash cloud over Europe during air space closure in April and May 2010, Atmos. Chem. Phys., 11, 2245–2279, doi:10.5194/acp-11-2245-2011, 2011.

Seinfeld, J. H. and Pandis, A. N.: Properties of the atmospheric aerosol, in: Atmospheric Chemistry and Physics – from Air Pollution to Climate Change, Chapter 8, John Wiley and Sons, New Jersey, United States of America, 350–394, 2006.

Sheehan, F. and Barclay, J.: Staged storage and magma recycling at Ambrym volcano, Vanuatu, J. Volcanol. Geoth. Res., doi:10.1016/j.jvolgeores.2016.02.024, online first, 2016.

Siebert, L., Simkin, T., and Kimberly, P.: Volcanoes of the World, 3rd Edn., Berkeley: University of California Press, United States of America, 568 pp., 2010.

Simpson, W. R., von Glasow, R., Riedel, K., Anderson, P., Ariya, P., Bottenheim, J., Burrows, J., Carpenter, L. J., Frieß, U., Goodsite, M. E., Heard, D., Hutterli, M., Jacobi, H.-W., Kaleschke, L., Neff, B., Plane, J., Platt, U., Richter, A., Roscoe, H., Sander, R., Shepson, P., Sodeau, J., Steffen, A., Wagner, T., and Wolff, E.: Halogens and their role in polar boundary-layer ozone depletion, Atmos. Chem. Phys., 7, 4375–4418, doi:10.5194/acp-7-4375-2007, 2007.

Simpson, W. R., Brown, S. S., Saiz-Lopez, A., Thornton, J. A., and von Glasow, R.: Tropospheric halogen chemistry: sources, cycling, and impacts, Chem. Rev., 115, 4035–4062, doi:10.1021/cr5006638, 2015.

Stevenson, D. S., Johnson, C. E., Collins, W. J., and Derwent, R. G.: The tropospheric sulphur cycle and the role of volcanic SO_2, Geol. Soc., London, Special Publications, 213, 295–305, 2003.

Stockwell, W. R., Kirchner, F., Kuhn, M., and Seefeld, S.: A new mechanism for regional atmospheric chemistry modeling, J. Geophys. Res.-Atmos., 102, 25847–25879, 1997.

Surl, L., Donohoue, D., Aiuppa, A., Bobrowski, N., and von Glasow, R.: Quantification of the depletion of ozone in the plume of Mount Etna, Atmos. Chem. Phys., 15, 2613–2628, doi:10.5194/acp-15-2613-2015, 2015.

Tabazadeh, A., Toon, O. B., Clegg, S. L., and Hamill, P.: A new parameterization of H_2SO_4/H_2O aerosol composition: Atmospheric implications, Geophys. Res. Lett., 24, 1931–1934, 1997.

Textor, C., Graf, H.-F., Herzog, M., and Oberhuber J. M.: Injection of gases into the stratosphere by explosive volcanic eruptions, J. Geophys. Res., 108, 4606, doi:10.1029/2002JD002987, 2003.

Theys, N., Van Roozendael, M., Dils, B., Hendrick, F., Hao, N., and De Mazière, M.: First satellite detection of volcanic bromine monoxide emission after the Kasatochi eruption, Geophys. Res. Lett., 36, L03809, doi:10.1029/2008GL036552, 2009.

Theys, N., De Smedt, I., Van Roozendael, M., Froidevaux, L., Clarisse, L., and Hendrick, F.: First satellite detection of volcanic OClO after the eruption of Puyehue-Cordón Caulle, Geophys. Res. Lett., 41, 667–672, doi:10.1002/2013GL058416, 2014.

Tie, X., Madronich, S., Walters, S., Zhang, R., Rasch, P., and Collins, W.: Effect of clouds on photolysis and oxidants in the troposphere, J. Geophys. Res., 108, 4642, doi:10.1029/2003JD003659, 2003.

Vance, A., McGonigle, A. J. S., Aiuppa, A., Stith, J. L., Turnbull, K., and von Glasow, R.: Ozone depletion in tropospheric volcanic plumes, Geophys. Res. Lett., 37, L22802, doi:10.1029/2010GL044997, 2010.

van der Werf, G. R., Randerson, J. T., Giglio, L., Collatz, G. J., Kasibhatla, P. S., and Arellano Jr., A. F.: Interannual variability in global biomass burning emissions from 1997 to 2004, Atmos. Chem. Phys., 6, 3423–3441, doi:10.5194/acp-6-3423-2006, 2006.

Vignelles, D., Roberts, T. J., Carboni, E., Ilyinskaya, E., Pfeffer, M., Waldhauserova, P. D., Schmidt, A., Berthet, G., Jegou, F., Renard, J. B., and Ólafsson, H.: Balloon-borne measurement of the aerosol size distribution from an Icelandic flood basalt eruption, Earth Planet. Sc. Lett., 453, 252–259, doi:10.1016/j.epsl.2016.08.027, 2016.

Voigt, C., Jessberger, P., Jurkat, T., Kaufmann, S., Baumann, R., Schlager, H., Bobrowski, N., Giuffrida, G., and Salerno, G.: Evolution of CO_2, SO_2, HCl, and HNO_3 in the volcanic plumes from Etna, Geophys. Res. Lett., 41, 2196–2203, 2014.

von Glasow, R.: Atmospheric chemistry in volcanic plumes, P. Natl. Acad. Sci. USA, 107, 6594–6599, 2010.

von Glasow, R., Bobrowski, N., and Kern, C.: The effects of volcanic eruptions on atmospheric chemistry, Chem. Geol., 263, 131–142, 2009.

Walko, R. L., Band, L. E., Baron, J., Kittel, T. G. F., Lammers, R., Lee, T. J., Ojima, D., Pielke Sr., R. A., Tayloer, C., Tague, C., Tremback, C. J., and Vidale, P. L.: Coupled atmosphere-biophysics-hydrology models for environmental modeling, J. Appl. Meteorol., 39, 931–944, 2000.

Wang, T. X., Kelley, M. D., Cooper, J. N., Beckwith, R. C., and Margerum, D. W.: Equilibrium, kinetic, and UV-spectral characteristics of aqueous bromine chloride, bromine, and chlorine species, Inorg. Chem., 33, 5872–5878, 1994.